INSTITUTO POLITÉCNICO DE BRAGANÇA
Escola Superior de Tecnologia e Gestão

Microencapsulation using alginate systems:

Spray-coagulation *versus* superhydrophobic surfaces approach

Diana Francisco Cuma

Final dissertation report submitted to

Escola Superior de Tecnologia e Gestão

Instituto Politécnico de Bragança

to obtain the Master Degree in

Chemical Engineering

Supervisor

Prof. Doutora Maria Filomena Barreiro

Co-Supervisor

Doutora Isabel Patrícia Fernandes

July 2018

“It always seems impossible until is done”

Acknowledgements

I would like to extend thanks to the many people, who so generously contributed for making this thesis possible.

I deeply express my gratitude to my supervisor Professora Filomena Barreiro, for all the support, teaching and patience given during this period. I will be eternally grateful for your gesture. I also want to thank my co-supervisor, Dr. Isabel Fernandes, for the support, patience, teaching, attention and the good friendship. I admire both of you.

Thank you also to Professor João Mano, from Universidade de Aveiro, for providing the superhydrophobic surfaces.

A special thanks to all my LSRE colleagues for all the support and encouragement, especially to Hélder, João, Catarina, Palloma and Samara, and also to Eng. Maria João Afonso from LPQ for help and sympathy.

To my dearest friends, Mila, Isabel and Cleide, for the love, encouragement, support and friendship.

To my friends Ana Rita, Rosa, Joeline, Nidaya and Stefan, for always being present.

A very special thank you to Cris, Madalina, Márcia, Carmen, Dicla, José, Michel, Micael and all the friends that Bragança offered me.

A special thanks to all the teachers who accompanied and encouraged me during my school journey.

Finally, my special thanks to my parents, for all the sacrifices that they made for me and for the support. To my sisters, aunts, uncles, cousins, godparents and family, thank you for all the support and encouragement.

Abstract

The use of biopolymers such as alginate has been growing in the last decades due to properties such as biocompatibility, non-toxicity and biodegradability. In this work the microencapsulation of a hydrophobic (curcumin) and a hydrophilic (safranin), used as model compounds with alginate matrices, was studied by comparing two encapsulation methods (spray coagulation and superhydrophobic surfaces) and by testing three calcium sources (calcium chloride, calcium gluconate and calcium lactate) to promote the alginate ionic crosslinking. The microspheres obtained through the spray/coagulation technique were characterized in terms of load, encapsulation efficiency and rehydration capacity. The release profiles of both active principles were evaluated. The results revealed that when calcium chloride is used a higher encapsulation efficiency was obtained (99.25% and 98.50%, respectively for curcumin and safranin), followed by calcium gluconate (98.45% and 97.55 for curcumin and safranin) and finally calcium lactate (97.91% for curcumin and 97.42 for safranin). Regarding the release profile, a lower release was achieved, for both compounds, when calcium chloride was used (5.70% of curcumin in ethanol medium, and 4.15% of safranin in distilled water), followed by the calcium gluconate crosslinked microspheres (8.3% for curcumin and 4.42% for safranin). Calcium lactate crosslinked microspheres give rise to the systems with higher release (12.1% for curcumin and 4.76% for safranin). The microspheres had a spherical conformation and the larger particle size (volume distribution) was obtained with the calcium gluconate-based systems (131.46, 78.85 and 91.46 μm for curcumin, safranin and empty microspheres, respectively). The calcium chloride-base systems give rise to the smallest ones (91.65, 60.10 and 80.31 μm, respectively for curcumin, safranin and empty microspheres). Through Fourier Transform Infrared Spectroscopy the contribution of the calcium source and the active principle on the microspheres spectra was identified, and thermogravimetric analysis evidenced an increasing of the thermal stability due to the alginate crosslinking effect, particularly when calcium chloride was used. Regarding the comparison of the two microencapsulated systems, the superhydrophobic surfaces showed a good performance having in view the encapsulation with alginate systems, since no loss of the active principle to the surface during the process was observed (qualitative

analysis). This constitute an advantage particularly for the case of the hydrophilic active principles.

Resumo

O uso de biopolímeros como o alginato tem aumentado nas últimas décadas devido a propriedades como biocompatibilidade, não-toxicidade e biodegradabilidade. Neste trabalho foi estudada a microencapsulação de uma substância hidrofóbica (curcumina) e uma hidrofílica (safranina), usadas como compostos modelo com matrizes de alginato, comparando dois métodos de encapsulação (spray/coagulação e superfícies superhidrofóbicas) e testando três fontes de cálcio (cloreto de cálcio, gluconato de cálcio e lactato de cálcio) para promover a reticulação iónica de alginato. As microesferas obtidas através da técnica de *spray*/coagulação foram caracterizadas em termos de carga, eficiência de encapsulação e capacidade de reidratação. Os perfis de liberação dos dois princípios ativos foram também avaliados. Os resultados revelaram que quando o cloreto de cálcio é utilizado se obtém maior eficiência de encapsulação (99,25% e 98,50%, respetivamente para curcumina e safranina), seguida do gluconato de cálcio (98,45% e 97,55 para curcumina e safranina) e finalmente lactato de cálcio (97,91% para curcumina e 97,42 para safranina). Quanto ao perfil de libertação, obteve-se uma libertação inferior, para ambos os compostos, quando se utilizou cloreto de cálcio (5,70% para a curcumina em etanol e 4,15% para a safranina em água), seguido das microesferas reticuladas com gluconato de cálcio (8,3% para a curcumina e 4,42% para a safranina). As microesferas reticuladas com lactato de cálcio originam os sistemas com maior capacidade de libertação (12,1% para a curcumina e 4,76% para a safranina). As microesferas possuem uma conformação esférica e o maior tamanho de partícula (distribuição de volume) foi obtido para os sistemas à base de gluconato de cálcio (131,46, 78,85 e 91,46 µm para curcumina, safranina e microesferas vazias, respetivamente). Os sistemas baseados em cloreto de cálcio originam os tamanhos menores (91,65, 60,10 e 80,31 µm, respetivamente para curcumina, safranina e microesferas vazias). Por espectroscopia no infravermelho com transformada de Fourier, foi identificada a contribuição da fonte de cálcio e do princípio ativo no espectro de microesferas e a análise termo gravimétrica evidenciou um aumento da estabilidade térmica devido ao efeito da reticulação, particularmente quando foi utilizado cloreto de cálcio. Quanto à comparação dos dois sistemas de microencapsulação, as superfícies superhidrofóbicas apresentaram um bom desempenho tendo em o uso de sistemas de alginato, uma vez que não foi observada perda do princípio ativo para a superfície durante o processo (análise qualitativa). Tal constitui uma vantagem particularmente para o caso dos princípios ativos hidrofílicos.

Table of contents

List of Figures

List of Tables

List of Abbreviations

(G) Guluronic acid

(M) Mannuronic acid

$CaCl_2$ Calcium chloride

Ca-glu Calcium gluconate

Ca-lact Calcium lactate

EE Encapsulation Efficiency

FDA Food and Drug Administration

FTIR Fourier-Transform Infrared Spectroscopy

GDL Glucono delta-lactone

GRAS Generally recognized as safe

MIC Microspheres

$M_{n.enc}$ Amount of non-encapsulated active principle

M_{theo} Theoretical amount of active principle

OM Optical Microscopy

PS Polystyrene

SH Superhydrophobic

TGA Thermogravimetric analysis

UV-vis Ultraviolet visible spectrophotometry

v/v Volume ratio

w/v Mass volume ratio

w/w Mass ratio

λ Wavelength

1.Introduction

1.1 Motivations and Objectives

The use of microencapsulation techniques allows the protection of active principles through the coating with polymeric materials, resulting in systems with improved stability and controlled release. However, the development of a microencapsulation chemical system, and the selection of a microencapsulation technique is not a simple task. The selection must considerer a broad range of factors, as for example the preservation of the active principle properties, and the compatibility with the type of polymeric material, which must be inert towards the active principle. Also, the application area for the developed microencapsulated products must also be taken in account.

Nowadays, the concern with the toxicity of chemicals and the search for green processes and chemical systems motivate the development of environmental friendly alternatives. In this sense, the selection of chemical systems based on biopolymers such as sodium alginate is a good option, and presently widely studied. However, there is a lack of information about the sodium alginate ionic crosslinking through different calcium sources, since a great part of the published studies use calcium chloride. In the same manner, and in a general way, the microencapsulation studies are focused on a particular active principle, around which the chemical system and process is developed. A lack of information is noticed regarding systematic studies focused on model compounds.

The use of encapsulation methods such as the spray-coagulation has a great advantage comparatively to other conventional process (ex. double emulsions) since it allows the microparticles production in a single step. Even though, the spray coagulation method has one major drawback related with the low encapsulation efficiency of hydrophilic substances that diffuses to the aqueous coagulation solution during the consolidation stage. Among the possible options for surpassing this disadvantage, the use of superhydrophobic surfaces for microencapsulation purposes is one of the latest adopted green alternatives. These surfaces are composed by hydrophobic coatings with a specific roughness that allow the formation of spherical aqueous droplets. This technique has as main advantages the individual solidification of spherical hydrogel droplets in a dry environment at room temperature and with high encapsulation efficiency.

Based on the aforementioned considerations, the present work has as main objective to study the microencapsulation of a hydrophilic and a hydrophobic model compounds,

using alginate systems by adopting and comparing two encapsulation methods: spray coagulation and superhydrophobic surfaces and testing three different calcium sources.

The selected hydrophobic model active principle was curcumin and the hydrophilic one safranin. Both active principle were colorants, and alginate was used as the matrix material. Two different microencapsulation processes: spray-coagulation and using superhydrophobic (SH) polystyrene surfaces. Moreover, the crosslinking of the resultant microdroplets using different calcium sources was tested, in order to evaluate the effect of the crosslinker chemical structure on the alginate coagulation/gelation. In this sense, calcium chloride ($CaCl_2$) , calcium gluconate (Ca-glu), and calcium lactate (Ca-lact) were tested.

The microspheres produced by the spray-coagulation method were characterized by optical microscopy (morphology), encapsulation efficiency (EE), load, dry residue, rehydration capacity, release profile, thermal properties (thermogravimetric analyis), chemical and structural characterization (FTIR) and particle size. For the microspheres produced by using the SH surface the characterization comprised only optical microscopy, dry residue and rehydration capacity.

1.2 Layout

The present thesis is divided in 5 main chapters:

- Chapter 1, “Introduction”, discusses the motivating and objectives of the present work, evidencing the novelty and interest of the theme;
- Chapter 2, “Bibliographic review”, gives a literature review of the main topics treated in this thesis;
- Chapter 3, “Materials and Methods” describes the materials used during this work, the microencapsulation methodologies, as well as the characterization methodologies;
- Chapter 4, “Results and Discussion”, presents the obtained results accompanied by a critical discussion;
- Chapter 5, “Conclusions and future work” contains the final considerations and the synthesis of the most relevant obtained results. Additionally, some future perspectives are stressed out.

Finally, Chapter 6 presents the bibliographic references supporting the present work

2. Bibliographic Review

2.1 Microencapsulation: General Concepts

Microencapsulation may be defined as the packaging of solids, liquid or gaseous materials within a polymeric coatings or matrix, forming small particles called microcapsules or microspheres, respectively (Silva et al., 2014). According to their size, the capsules are classified as nanoparticles or microparticles, ranging from 0.01 to 0.2 μm and from 1 to 100 μm, respectively. Above 100 μm they are called macroparticles (Meier, 2015)

The term "microcapsule" is used to define the spherical particles, constituted by an inner core, which contains an active principle coated by a polymer layer of variable thickness. On the other hand, microspheres are equally spherical particles, constituted by a polymer network (matrix) in which the active substance is distributed in solid particles or molecular state. However, the terms "microsphere" and "microcapsule" are used regularly as synonyms (Singh et al., 2010). Figure 1 shows the different structures of microcapsules and microspheres.

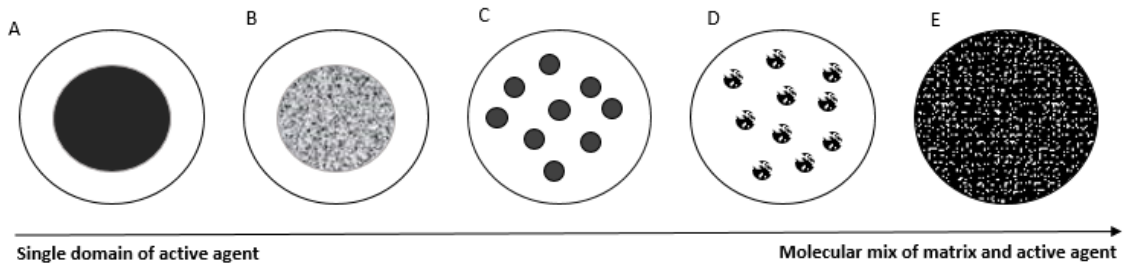

Figure 1 Different structures of microcapsules and microspheres: A- Microcapsule with solid core; B- microcapsule with non-solid core; C- Microcapsule with solid microdomains or nanodomains; D- Microcapsule with non-solid microdomains or nanodomains; E- Microsphere with molecular mix of matrix and encapsulated agent (Redraw from Singh et al.,2010).

For the microcapsules, the polymer acts as a protective film, isolating the core (active principle) and avoiding the effect of its inadequate exposure. This membrane can dissolve and/or disrupt itself through specific stimulus, releasing the core at the desired place or at the ideal time (Silva et al., 2014) .

Generally, there are three different mechanisms to promote the core release from the microcapsule: mechanical rupture of the wall, dissolution or melting of the wall and diffusion trough the wall. Ablation (slow erosion of the shell) and biodegradation are also included, but they are less common mechanisms (Dubey et al., 2009). Due to mechanical

breakage of the shell (that not occurs simultaneously for all particles), it is possible to achieve a controlled release, mechanism very useful for some applications (Rodrigues et al., 2009).

In microsphere systems, the release is mostly achieved by diffusion of the core material within the matrix. The rate of release can be influenced by the crosslinking degree of the matrix materials, as well as by the swelling imparted by a surrounding solvent (Singh et al., 2010).

Microencapsulation can also be used to convert liquids into solids (Gharsallaoui et al., 2007), provide environmental protection (Kailasapathy, 2002) and controlling the release characteristics of an active principle (Quinlan et al., 2017). Several of these properties can be attained by macro packaging techniques, however, the singularity of microencapsulation is the reduced size of the produced particles, which offers the possibility to be used and/or adapted to a wide variety of final applications (Agnihotri et al., 2012).

Microencapsulation becomes an important issue, not only to protect sensitive substances from the external environment, but also to mask the organoleptic properties (e.g. color, taste and odor). Control these characteristics is very important particularly in the food and cosmetic sectors (Dias et al., 2015). Also, microencapsulation can provide a way for safe handling of toxic materials (Jyothi et al., 2010).

Currently microencapsulation can be used in several applications. Figure 2 shows the use of the process according to different areas (drugs, food, cosmetic, textile, electronics, agriculture and biomedical). It can be observed that the major sector of application for microencapsulation is in the pharmaceutical sector (drugs), followed by the food area and then cosmetics. The least volume of application of this process is observed in the electronics sector.

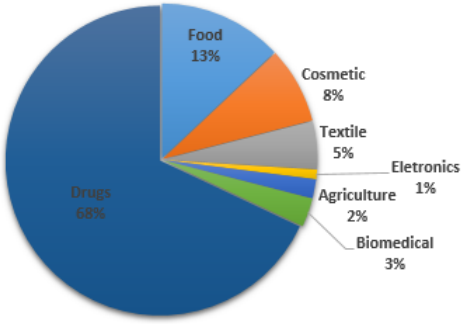

Figure 2 Schematic representation of the statistical distribution of microencapsulation over different fields of application (obtained on ISI web of knowledge, April 2013. Redrawn from (Martins et al., 2014).

2.2 Coating Materials

The selection of an appropriate coating material decides the physical and chemical properties of the resultant microcapsules (Singh et al., 2010)**.** The coating material should be capable to create a film with a good cohesion towards the core material, be chemically compatible and nonreactive with the core material and provide the desired coating properties, such as strength, flexibility, impermeability, optical properties and stability. Also, the coating material should provide the stabilization of the core material, controlled release under specific conditions and be soluble in a specific solvent or aqueous media. Generally, hydrophilic and hydrophobic polymers or a combination of both are used (Agnihotri et al., 2012). Table 1 shows some coating materials used in microencapsulation processes, where the following classes are considered: carbohydrates, gums, lipids, natural polyesters, synthetic polymers and proteins. According to Estevinho et al., (2013), the most used polymers as encapsulating agents are: cellulose, acetophtalat, alginate, arabic gum, chitosan, ethyl cellulose, gelatin, K-carrageenan, maltodextrin and starch. Among them, and due to the easy application and non-toxicity, alginate offers many advantages for applications in different industrial fields.

Table 1 Coating materials used in microencapsulation (Meier, 2015)

Carbohydrates	Starch, dextrin, different sugars, chitosan and cellulose.
Gums	Arabic gum, alginate and carrageenan.
Lipids	Wax, paraffin, stearic acid, monoglycerides and diglycerides.
Natural polyesters	Polyhydroxyalkanoates, as poly (3-hydroxybutyrate) P (3HB) or poly (3-hydroxyvaleric) P (3HV) and copolymers.
Synthetic Polymers	Polyacrylates, polyurethanes and phenol-formaldehyde resins.
Proteins	Gluten, casein, gelatin and albumin.

2.2.1 Alginate

Alginate is a linear copolymer composed by (1, 4)-linked-β-D-mannuronic (M) and α-L-guluronic (G) acid blocks. The blocks are disposed in consecutive G residues, consecutive M residues and alternate M and G residues, as shown in Figure 3 (Lee and Mooney, 2012). Alginate has a molecular weight of 216.12 g/mol and is identified by IUPAC as sodium 3,4,5,6-tetrahydroxyoxane-2-carboxyate. It has a water solubility of 782 g/L, and is soluble in alcohol, chloroform and other organic solvents. The pKa is different for each alginate group: 3.65 for the M, and 3.38 for the G moieties (Mchugh, 2013).

This compound is produced from two sources, algae and bacteria. The commercially available alginates are derived primarily from brown algae (e.g. *Macrocystis pyrifera*). The ones that are isolated from bacteria such as *Azotobacter* and *Pseudomonas* species are usually not economically viable for commercial applications and confined to small-scale research studies (Goh et al., 2012).

The extraction process of alginate from seaweeds is not complicated, but comprises multistage processes, starting usually with the treatment of the dried raw material using diluted mineral acid. After the purification, the obtained alginic acid is converted into a water-soluble sodium salt in the presence of calcium carbonate, which is next transformed back into the acid or salt form (Figure 4) (Szekalska et al., 2016)

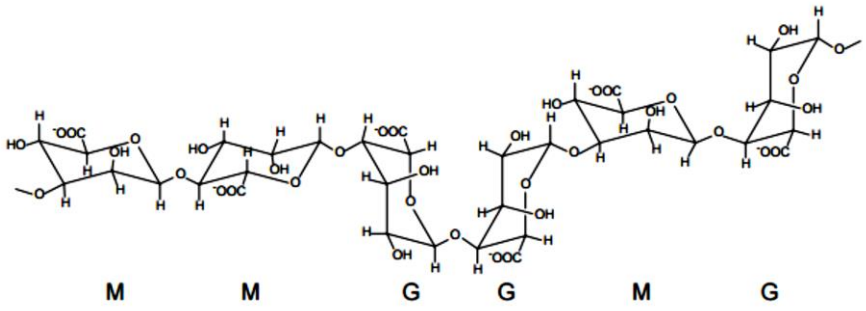

Figure 3 Polymeric chain of alginate composed by (M) blocks, (G) blocks and (MG) blocks (Daemi et al., 2013).

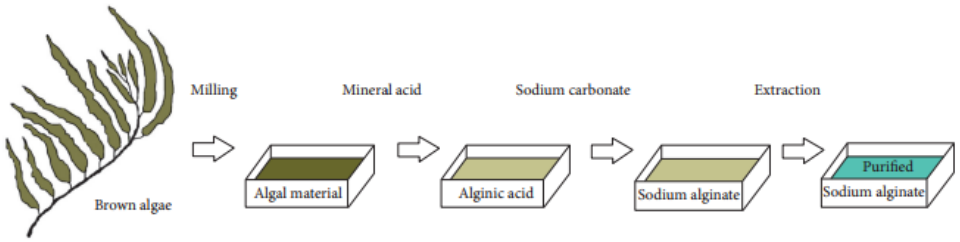

Figure 4 Procedure of sodium alginate extraction (Szekalska et al., 2016).

This biopolymer has numerous applications in biomedical science and engineering, due its favorable properties, including biocompatibility and easy of gelation (Lee and Mooney, 2012). Alginates are used as stabilizers and thickeners for a wide range of products. The functional role of alginate in some common applications is summarized in Table 2.

Table 2 Applications of alginate in different industries. Adapted from Goh et al. (2012).

Applications	Function
Food and beverage industry	
Drinks, Ice-cream, Jelly	Stabilizers, thickeners
Ethanol production	Encapsulation material of yeast cells
Pharmaceutical industry	
Cell culture and transplantation	Encapsulation material
Dental impression material	Mold material
Pills	Adhesive agent, sustained release
Wound dressing	Hemostatic and absorbent
Other industries	
Fabrics	Thickeners
Paper	Adhesive and suspending agent
Toothpaste	Stabilizers, thickeners

Alginate is characterized by the following properties:

Solubility: the solubility of alginate in water is influenced by three factors: pH of the solvent, ionic strength of the medium and the presence of gelling ions in the solvent. To make alginate soluble it is essential that the pH is above a certain critical value (pKa) and the carboxylic acid groups be deprotonated. Changing the ionic strength of the medium affects the properties such as polymer conformation, chain extension, viscosity and therefore the solubility (Pawar and Edgar, 2012).

Biocompatibility: Tam reported that the biocompatibility of alginate gels is influenced by the proportion and distribution of the M and G residues within the alginate backbone,

as well at by its intrinsic viscosity (Tam et al., 2011). Alginates are included in a group of compounds that are generally regarded as safe (GRAS) by the FDA (George and Abraham, 2006).

pH: The behavior of alginate varies according to the pH to which it is exposed. A rapid decrease of pH results on the precipitation of alginate molecules in the form of aggregates, while a slow and steady drop of the pH results in a gelatinous precipitate of alginate molecules. The dependence of viscosity from pH medium is unaffected in the range comprised between5-11. An increase of pH above 10 results in a slow depolymerization process (Ching et al., 2017a; Mchugh, 2013) .

2.2.2 Alginate crosslinking

Currently, there are various approaches to crosslink alginate, such as covalent crosslink (Rouillard et al., 2011) and enzymatic crosslinking (Hou et al., 2015), however, ionic crosslinking is the most common method to prepare alginate hydrogels (Lee and Mooney, 2012).

According to Russo et al. (2007), the alginate affinity towards divalent cations decreases in the following order: Pb>Cu>Cd>Ba>Sr>Ca>Co, Ni, Zn>Mn. Alginate crosslinking can be achieved by interaction with divalent cations such as Mg^{2+} (Topuz et al., 2012) , Ba^{2+} and Sr^{2+} (Mørch et al., 2006). However, the use of this compounds has some restrictions, being this related with the concentration required for an effective crosslinking. For example, in the case of Mg^{2+} the ion required concentration is 5-10-fold higher than the one reported for calcium-based salts. Moreover in this case the gelation process is very slow, it can take 2-3 hours (Topuz et al., 2012). Ba^{2+} and Sr^{2+} are also used, but at low concentrations, due to their mild toxic characteristics (Ching et al., 2017b).

Ca^{2+} is the most used cation for alginate crosslinking due to the mild reaction conditions. The alginate crosslinking with calcium ions is achieved by the ionic interaction between calcium ions and the carboxyl groups of the guluronic acid residues of two neighboring alginate chains, resulting on a stable three-dimensional network, named the “egg-box” model, represented in Figure 5 (Rao, J. K., & Rao, 1997).

Considering the alginate crosslinking, the gelation method can be classified as external or internal, by using ionic crosslink agents, such as calcium salts (Chan et al., 2006; Lee

and Mooney, 2012). Regarding the alginate beads internally crosslinked, they can be prepared by the emulsification/gelation technique, where, the alginate mixed with calcium salt solution is dropped into an oily phase. After, the pH is decreased, usually by adding an acid solution, in order to release the calcium ions for further reaction with the alginate, resulting in the alginate beads gelification (Poncelet et al., 1995; Silva et al., 2006). Alternatively to the acid solution glucono delta-lactone (GDL) can be added to the alginate phase, which slowly lowers the pH inside the alginate bead, allowing the calcium ions to be released (Paques et al., 2013). Regarding the alginate beads preparation by external crosslinking, herein the alginate solution is dripped into a calcium salt aqueous solution, and the gelation is achieved by the diffusion and reaction of the calcium ions into the alginate bead. Some of the methods using this technique are spray-coagulation (Rached et al., 2016) and ionic gelation (Rakesh et al., 2015).

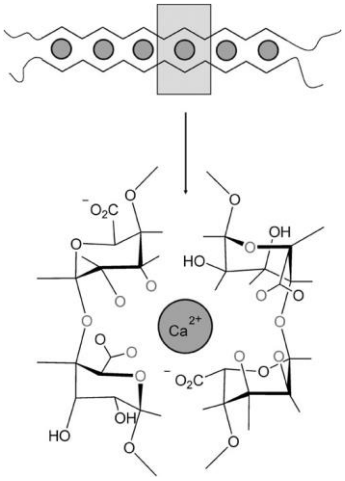

Figure 5 Schematic drawing of the "egg-box" model for alginate formation (Leick et al., 2010).

2.2.2.1 Calcium Sources

The alginate crosslinking by Ca^{2+} has been widely used due its high biocompatibility, relatively low cost, reduced immunogenicity and capacity to form hydrogels under gentle conditions (Galateanu et al., 2012). The use of calcium salts has been evaluated more detailed since the resulting gels became useful for both food and non-food systems (Clare, 2012). The chemical reaction between sodium alginate and the calcium ions is dependent on the solubility and the concentration of the calcium ions. These parameters will influence the structure and the performance of the microspheres.

Calcium chloride ($CaCl_2$) is an inorganic salt, highly soluble in water, usually used as a supplemental source of calcium to treat calcium deficiency in humans (Trailokya et al.,

2017). This compound can also be used to treat magnesium intoxications, caused by overdose of magnesium sulfate (Intensive and Unit, 2012). $CaCl_2$ is one of the most frequently used agents to promote the ionic crosslinking of alginate, however, it is often described as leading to a rapid and poorly controlled gelation, partly due to its high solubility in aqueous solutions (Lee and Mooney, 2012). This is an advantage because the rapid gelation decreases the preparation time, ensures a consistent product and can reduce the loss of hydrophilic active principles for the outer aqueous medium.

Calcium lactate (Ca-lact) is a water soluble organic salt, composed by two lactate anions per each calcium cation (Figure 6). It is widely used for the treatment of calcium deficiency (Straub, 2007), as a food additive (Silva and Lidon, 2016) and for water treatment (Bustos and Cruz, 2012). The use of calcium lactate for alginate crosslinking has been reported in few studies, comparatively with $CaCl_2$ (Devatkal and Mendiratta, 2001; Lee and Rogers, 2012). Calcium lactate can be associated with calcium gluconate (calcium glucono-lactate) in order to increase the Ca^{2+} concentration and the solubility, due their low concentrations of elemental Ca^{2+}. The solubility is enhanced to approximately 400 g/L in water, comparatively with the one of the pure components (see Table 3).

Calcium gluconate (Ca-glu) is a mineral supplement used in pharmaceutical industry, also used as treatment for calcium deficiency, namely hypercalcemia (Ramachandran et al., 2006). It has a low solubility in water, being dependent of the temperature, and is insoluble in alcohols and other organic solvents (Lee and Rogers, 2012; National Institutes of Health, 2016). Giunchedi et al., (2000) studied the controlled release of ketoprofen using alginate as the matrix material and calcium gluconate as the alginate crosslinker. Their results showed that the presence of calcium gluconate in combination with sodium alginate, led to an enhancement of the release rate from the produced matrices, and also to a constant release rate of the drug.

Lee and Rogers, (2012) studied the behavior of alginate microspheres crosslinked with the three sources of calcium mentioned above. The study was focused in the gelation rate and the hardness developed by the developed alginate microspheres. The results showed that $CaCl_2$ is the best option to crosslink alginate due to its rapid dissociation and high solubility. The use of calcium gluconate can be advantageous to manipulate the membrane thickness, due to its slow gelation rate (comparatively with $CaCl_2$). By

comparing the gelation time, $CaCl_2$ takes approximately 100 s to crosslink the alginate, followed by proximately 500 s for the Ca-lact, and approximately 3000 s for the Ca-glu.

Calcium carbonate is widely used to crosslink alginate by internal gelation method (Jang et al., 2014; Silva et al., 2006), due to its low solubility in water. This compound is soluble in water under acidic conditions, and some studies reported an increase of solubility with the water temperature decrease, i.e., it is maximized in cold water (10ºC) (Dabb, 1971). Silva et al. (2006) described the production process of alginate microspheres loaded with insulin for oral administration, using the internal gelation method. The authors reported that the microspheres had a mean diameter lower than 60 μm and an encapsulation efficiency around 75%. Internal gelation may provide an alternative method to produce microspheres using minor amounts of calcium salts (Chan et al., 2002). Table 3 presents a survey of the three crosslinkers physico-chemical properties and Figure 6 shows the chemical structures, respectively, for the following calcium salts: Calcium chloride, Calcium gluconate and Calcium lactate.

Table 4 shows a review of the published studies using calcium chloride, calcium gluconate and calcium lactate as alginate crosslinking agents, as well as the used process conditions.

Table 3 Physico-chemical properties of the calcium salts

Crosslinking agents	**Chemical formula**	**MM (g/mol)**	**Solubility/ Solvent**	**pH**	**pKa**	**Elemental Ca^{2+}**
Calcium chloride dihydrate	$CaCl_2.2H_2O$	147.01	1208 g/L, H_2O	4.5 - 8.5 (H_2O, 20ºC)	-7	21 % per 1 gram of salt
Calcium D-gluconate monohydrate	$C_{12}H_{22}CaO_{14}.H_2O$	448.39	30g/L, H_2O	6.6 (H_20, 20ºC)	3.70	9% per 1 gram of salt
Calcium L-lactate hydrate	$C_6H_{10}CaO_6.xH_2O$	218.22	50 g/L, H_2O	6.0 - 8.0 (H_2O, 20ºC)	3.78	13% per 1 gram of salt

Table 4 Review of studies using calcium sources to crosslink alginate

Crosslinker	Crosslinking Process	Concentrations	Process conditions	References
$CaCl_2$	Ionic crosslinking	$CaCl_2$: 1-3% (w/v); Alginate: 2-2.5% (w/v); TMZ[1]: 2-3% (w/v);	Crosslinking time: 1 hour;	(Mandal et al., 2010)
	Ionic crosslinking	$CaCl_2$: 2%(w/v); Alginate: 1% (w/v);	Crosslinking Time: 30 min; Dissolution Temp. of alginate: 70-75ºC	(Russo et al., 2007)
Ca-Glu	Ionic crosslinking	Ca-Glu: 4.5% (w/v) Alginate: 1.5% (w/v)	Crosslinking Time:30 min;	(Fravel, 1985)
	Ionic crosslinking	Ca-Glu: 7% (w/v) Alginate: 4% (w/v) *M. brunneum: 1% (w/w)*	Crosslinking Time:2-10 min;	(Humbert et al., 2017)
Ca-Lact	Ionic crosslinking	Ca-Lact: 2% (w/v) Alginate: 2 % (w/v)	Crosslinking Time: 30 sec.	(Kampf and Nussinovitch, 2000)
	Ionic crosslinking	Ca-Lact: 2% (w/v) Alginate: 2 % (w/v)	Crosslinking Time: 2-10 min;	(Tsai et al., 2017)

1- Trimetazidine dihydrochloride

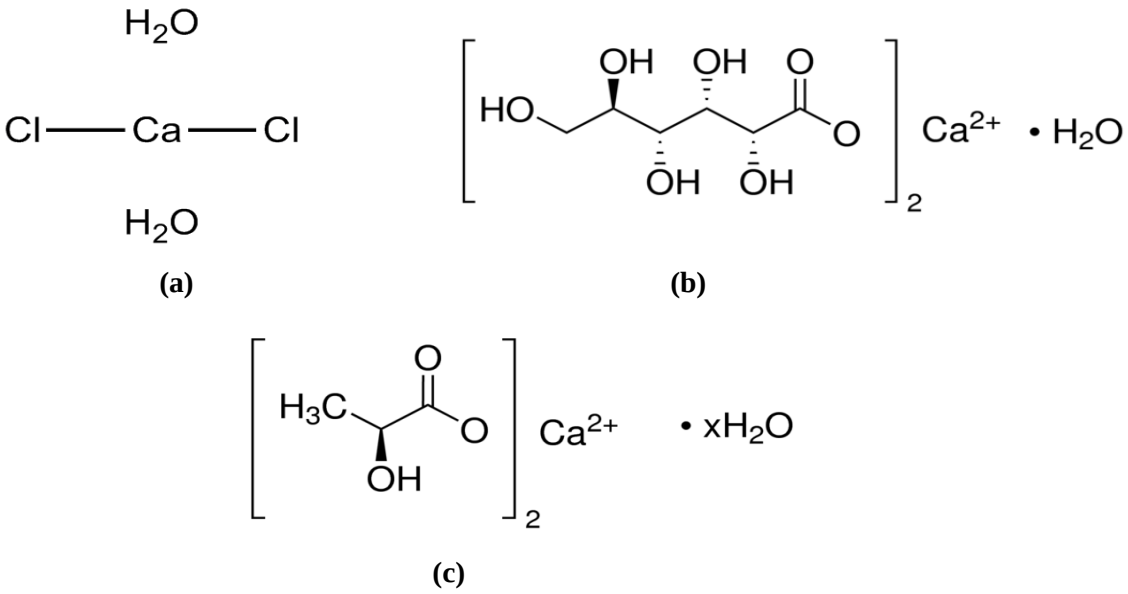

Figure 6 Chemical structures of calcium chloride (a), calcium gluconate monohydrate (b) and calcium lactate hydrate (c).

2.3 Overall of existing microencapsulation techniques

Currently, there are several methods that can be used for microencapsulation. The selection of a specific method should be according to the final application that will be given to the microcapsule, the desired size and the physico-chemical properties of the active principle and of the encapsulated material to be used (Matté and Da Rosa, 2013). According to Ghosh, (2006), microencapsulation techniques can be divided into two basic groups, namely chemical and physical methods, with the latter being further subdivided into physico-chemical and physico-mechanical techniques. Following this classification, Table 5 summarizes some of the most important microencapsulation processes.

Table 5 Different techniques used for microencapsulation (Adapted from Gosh,2006).

Chemical Methods	**Physical Methods**	
	Physico-mechanical	Physico-chemical
Poly condensation	Spray-drying	Coacervation
Interfacial polymerization	Multiple nozzle spraying	Layer-by-Layer (LBL) assembly
Suspension, dispersion and emulsion polymerization	Fluid-bed coating	Supercritical CO_2-assisted microencapsulation

Even with a large variety of microencapsulation techniques, no single method is appropriate to encapsulate different types of active principles. It depends, among other factors, upon the type of the core material, the size required for the particle, the permeability of the wall and the variable properties of the microcapsule. The process must be optimized to provide a satisfactory quality of the desire product. Table 6 shows an overview of the particle's size obtained according to different techniques.

Table 6 Microencapsulation processes with their relative particle size ranges. Adapted from Gosh (2006).

Microencapsulation Process	**Particle size (μm)**
Extrusion	250-2500
Spray-drying	5-5000
Coacervation	2-1200
In-situ polymerization	0.5-1100
Layer-by-layer (LbL) assembly	0.02-20
Interfacial polymerization	0.5-1000
Sol-gel encapsulation	2-20

According to Agnihotri et al (2012), The fabrication of microcapsules has to obey to certain specifications, namely:

- The ability to incorporate reasonably high concentrations of the active principle;
- Stability of the preparation after synthesis with an adequate shell life;
- Controlled particle size and dispersability in aqueous vehicules or others depending on the application;
- Release of the active principle with a good control and an appropriate time scale;
- Biocompatibility with controlable susceptibility to chemical modification.

Currently, there are several methods to apply microencapsulation using alginate, such as vibrating nozzle and coaxial gas flow extrusion (Koch et al., 2003), emulsification (Chan et al., 2002) and spray drying (Szekalska et al., 2016). There is a variety of processes related with "spray" methods, such as spray drying (Jyothi et al., 2010), and also atomization (spray) followed by coagulation.

2.3.1 Spray-coagulation method

Spray-coagulation, or atomization/coagulation, consists in a techinique where a solution of the polymeric material toghether with the active principle is atomized using an atomization system, e.g the apparatus Nisco Var J30 (Figure 7), followed by microsphere's consolidation upon contact with a bath containing the crosslinking agent. After a certain contact time, the microspheres can be colected by a decantation or filtration process, depending on the microspheres sizes. In a general way, one of the main advantages of using spray-coagulation techniques is the non-use of high temperatures like in spray-drying method, which can compromise the encapsulation of thermosensive substances, commonly associated with various natural compounds.

Rached et al., (2016) described the process for the microencapsulation of *Ceratonia siliqua L* extract with sodium alginate. The solution containing the alginate and the extract was atomized using the Nisco Var J30 system to produce the microspheres. The atomized microspheres were coagulated using a calcium chloride aqueous solution, for 4 hours. Posteriorly, the microspheres were collected by filtration and washed with distillated water. The microspheres were produced with diferent ratios extract/alginate, and the results showed an encapsulation efficiency around 100% for all the tested products.

In Table 7, some works using alginate and spray-coagulation technique are sumarized, putting in evidence the character of the encapsulated active principle (hydrophilic or hydrophobic) and the achieved encapsulation efficiency.

Figure 7 Nisco Var J30 system.

Table 7 Reports using spray-coagulation method with alginate systems.

Active Principle	Hydrophobic/Hydrophilic character	Coagulation Agent and time	Encapsulation Efficiency	References
Rubus ulmifolius Schott	As a methanolic extract - Hydrophilic	$CaCl_2$; 4 hours	~100%	(Martins et al., 2014)
Catechin	As a methanolic extract Hydrophilic	$CaCl_2$; 4 hours	87%	(Viegas et al., 2013)
Rosa micrantha	As a ethanolic extract - Hydrophilic	$CaCl_2$; 4 hours	53.3%	(Viegas, 2013)
Fragaria vesca L.	As a ethanolic extract - Hydrophilic	$CaCl_2$; 4 hours	95%	(Dias et al., 2015)

2.4 Applications of Microencapsulation

One of the main objectives of microencapsulation is not only to isolate the core from the surrounding environment, but also to control the rate at which it leaves the microcapsule (controlled release). Examples include the controlled release of citric acid in the food industry (Soccol et al., 2006), chemical drugs in the pharmaceutics industry (Farazuddin et al., 2011) and fertilizers in the agro-industry (Tsuiji, 2001). Currently, any industrial area could beneficiate from microencapsulation technologies, being pharmaceutical and food industry the main driving forces for microencapsulation advances (Paulo and Santos, 2017).

2.4.1 Agriculture

Microencapsulation process has gained huge interest in several areas, including agriculture, particularly for crops protection. Nowadays, insect pheromones are becoming viable as a biorational alternative to conventional hard pesticides. As an example, polymer microcapsules (polyuria, gelatin and gum Arabic) serve as efficient vehicles to deliver the pheromone by spraying the capsule dispersion. Further, encapsulation protects the pheromone from oxidation and light during storage and release (Dubey et al., 2009).

2.4.2 Pharmaceutics

One of the major areas of application of the encapsulation technique is pharmaceutical/ biomedical in order to achieve controlled/sustained drug delivery. Controlled drug delivery technology represents one of the frontier areas of science, which involves multidisciplinary scientific approaches, contributing for human health care. These delivery systems offer numerous advantages compared to conventional dosage forms, which include improved efficacy, reduced toxicity, and improved patient compliance and convenience, with the advantage to choose of the right biodegradable polymers (Singh et al., 2010). With these systems, microparticles sensitive to the biological environment are designed to deliver an active drug in a site-specific way (stomach, colon, specific organs). One of the main advantages of such systems is to protect sensitive drugs from drastic environment (pH, temperature etc.) and to reduce the number of administrations for patients (Jyothi Sri et al., 2012).

2.4.3 Food Industry

The microencapsulation technology has been used by the food industry for more than 60 years. (Desai and Park 2005). According with Poshadri and Kuna (2010), microcapsules offer to food processors a means to protect sensitive food components, avoiding nutritional loss, incorporate unusual or time-release mechanisms into the formulation and mask or preserve flavors and aromas. In addition, microencapsulation can simplify the food manufacturing process by converting liquids to solid powders, decreasing production costs allowing batch processing using low cost, powder handling equipment.

2.5 Microencapsulation of hydrophilic and hydrophobic compounds

The use of biodegradable polymers like sodium alginate, carrageenan and pectin has gained a wide acceptance in the development of controlled drug delivery systems. Classically, hydrogels have been used to delivery small hydrophilic drugs, which have high solubility in the hydrogel and in water (Ghosal and Ray, 2011; Hoare and Kohane, 2008). Due to the affinity with the aqueous medium, a low encapsulation efficiency's is expected, and consequently a high release rate of the substance, if final application comprises aqueous systems.

Several vitamins (such as vitamin A and D), antioxidants (curcumin, carotenes) and a great part of the newly developed drugs are hydrophobic substances. The poor water solubility is a limiting factor to their delivery using the conventional formulations (Josef et al., 2013). These restrictions have prompted researchers to develop novel formulations based on the incorporation of the hydrophobic compound into biocompatible organic substances like liposomes, polyethylene glycols, biopolymers and celluloses. Encapsulation in surfactant micelles, polymeric micelles, nanoparticles, phospholipids, cyclodextrins, hydrogels and liposomes can be the solution to overcome these limitations. In the present work, an approach based on model compounds is adopted. In this sense safranin is going to be used as a hydrophilic model active principle and curcumin as the hydrophobic one.

2.5.1 Safranin

Safranin O, or basic-red 2, is a biological stain, used in cytology and histology. The best-known application of safranin is in Gram and endospore staining. Safranin is a phenazine dye, which is similar to other planar dyes with chemical structures classified in the acridine, thiazine and xanthene groups. Phenazines derivatives are known to inhibit bacterial grow (Heli et al., 2007). Safranin is dark granulated powder in the solid state that becomes a red in aqueous medium (Figure 8). It has a molecular weight of 350.85 g/mol, chemical formula $C_{20}H_{19}ClN_4$ and is identified by IUPAC as 3,7-dimethyl-10-phenylphenazine-10-ium-2,8-diamine;chloride (PubChem, 2018). Safranin is soluble in water and ethanol and it has a maximum absorption in the visible region ranging from 517 nm to 530 nm.

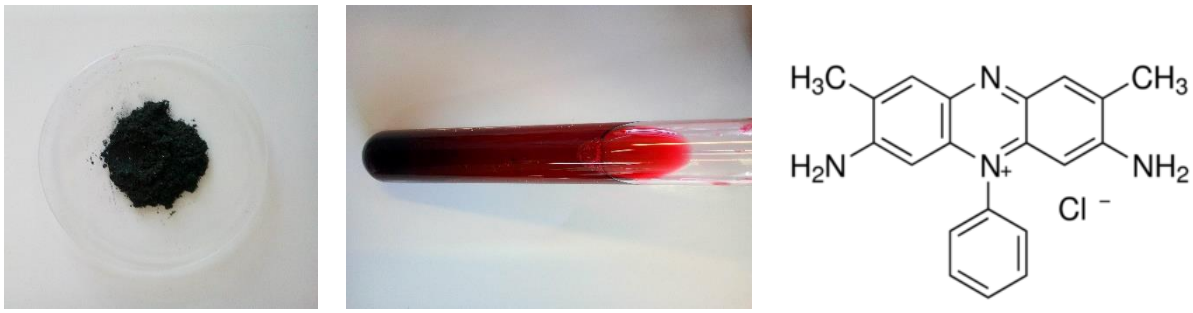

(a) (b) (c)

Figure 8 Safranin O: (a) solid state; (b) aqueous medium; (c) chemical structure.

2.5.2 Curcumin

Curcumin is derived from the turmeric plant (*Curcuma longa linn*), is a gold-colored spice commonly used in India subcontinent and Asian countries cuisine. Turmeric's plant is a short-stemmed perennial herb, member of the ginger family that grows throughout the Indian subcontinent and tropical countries, particularly Southeast Asia. *Curcuma longa* is used traditionally in Asian countries as a medicinal herb due to its anti-oxidant, anti-inflammatory, anti-mutagenic, antimicrobial and anticancer properties (Hewlings and Kalman, 2017). The rhizomes of the plant, also referred as the root, is the most used part of the plant (Figure 9).

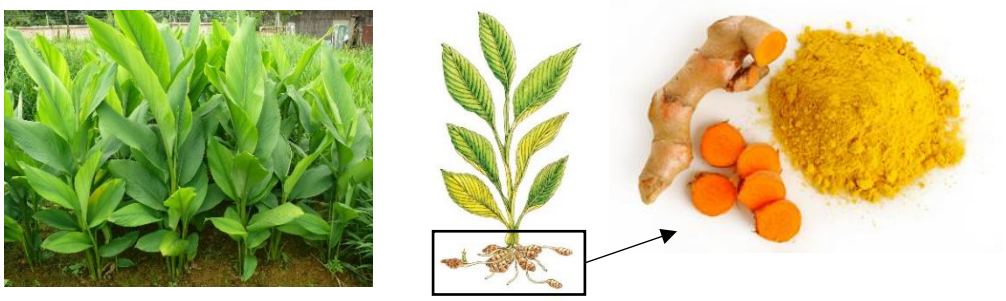

Figure 9 *Curcuma longa* and the rhizomes.

Due to the above mentioned interesting properties of curcumin, in the last decade, about two hundred papers and approximately one hundred patents concerning curcumin were published annually (Grynkiewicz and Ślifirski, 2012). Since Vogel and Pelletier reported the extraction of curcumin from turmeric, more advanced and improved methods have been developed to separate this compound.

Curcumin is recognized and used worldwide in many different forms due the multiple health benefits. Curcumin is applied in food industries as food additive, flavoring and preservative. This compound is listed in the International Numbery System for food additives (INS) as a safe coloring agent, with the code E100. Curcumin is considered a GRAS by the FDA due to its low toxicity, even when ingested at relatively high levels (Hewlings and Kalman, 2017; Strimpakos and Sharma, 2008; Zheng et al., 2017).

It has been shown that curcumin exhibit a range of pharmacological activities, including anti-inflammatory, anti-oxidant, anti-proliferative, anti-carcinogenic and anti-microbial (Song et al., 2012). The main restrictions of using curcumin is related to its poor aqueous solubility, stability and consequently bioavailability. (Anand et al., 2007; Mondal et al., 2016).

Curcumin, also known as curcumin I or diferuloylmethane, is a phytochemical and polyphenolic compound that occurs naturally from the rhizome of turmeric, along with other curcuminoids. This compound was isolated in 1815 and obtained in the crystalline form by Daube in 1870 and identified by IUPAC as (1E,6E)-1,7-bis-(4-hydroxy-3-methoxyphenyl)-1,6-heptadiene-3,5-dione, or diferuloylmethane (Lin, 2007; Mondal et al., 2016)

Curcumin is a symmetric molecule composed by two ferulic acid molecules linked by a methylene bridge at the carbon atoms of the carboxyl groups (Figure 10). The absorption spectrum of curcumin has two strong absorption bands, one in the visible region with a maximum ranging from 410 to 430 nm and another in the UV region with a maximum at 265 nm region (Priyadarsini, 2014). The major curcuminoids present in turmeric are diferuloylmethane (curcumin I), demethoxycurcumin (curcumin II), bisdemethoxycurcumin (curcumin III) and recently identified cyclocurcumin. Commercial curcumin contains approximately 77% of diferuloylmethane, 17% of demethoxycurcumin and 6% of bisdemethoxycurcumin (Anand et al., 2007; Grynkiewicz and Ślifirski, 2012). Table 8 presents some physico-chemical properties of the curcumin and safranin.

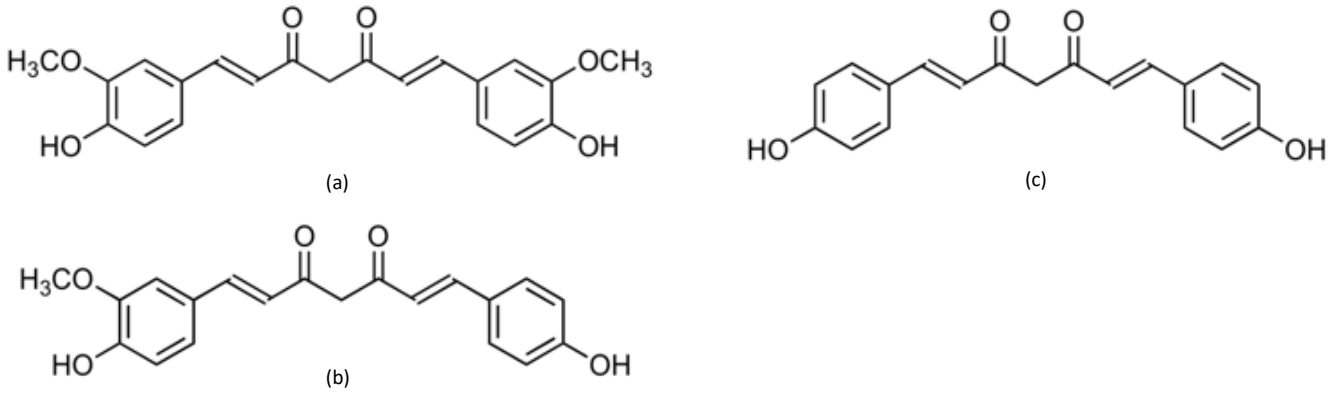

Figure 10 Structure of natural curcumins derivates, curcuminoids: (a) Curcumin; (b) demethoxycurcumin; (c) bisdemethoxycurcumin.

Table 8 Physico-chemical properties of curcumin and safranin.

Substance	**Chemical formula**	**MM (g/mol)**	**Solubility**	**pKa**
Safranin O	$C_{20}H_{10}ClN_4$	350.84	50 g/L, H_2O Soluble in ethanol	6.4
Curcumin	$C_{21}H_{20}O_6$	368.38	Soluble in ethanol and other organic solvents	pKa_1-7.8 pKa_2-8.5 pKa_3-9.0

2.6 Microencapsulation based on superhydrophobic surfaces

Many surfaces in nature are highly hydrophobic and self-cleaning. Examples include the wings of butterflies and red rose's petals, as shown in Figure 11. The best-known example of a hydrophobic self-cleaning surface is the lotus flower leaves. Biologically inspired design, adaptation or derivation from nature is usually referred as "biomimetic" (Subhash Latthe et al., 2012). Based on this concept, researchers have developed and implemented processes to treat surfaces in order to confer that characteristics.

(a) (b) (c)

Figure 11 Natural superhydrophobic surfaces: (a) Lotus leaf; (b) Red rose petals; (c) Butterfly's wings.

A superhydrophobic surface is a surface where a drop of water forms an almost perfect sphere and even a very slight tilting is sufficient to cause the water drop to roll off (Li et al., 2007; Subhash Latthe et al., 2012). Superhydrophobicity is the enhancement of hydrophobic properties due to the roughness. The effect of rougheness-induced superhydrophobicity was firstly described by Robert Wenzel in 1930's. A hydrophobic surface with a contact angle $\theta>90^{o}$ becomes superhydrophobic after a roughening process, with contact angles higher than 150^{o} (Nosonovsky and Bhushan, 2009).

These surfaces have gain a special attention because some properties are expected, such as anti-contamination, anti-sticking and self-cleaning (Li et al., 2007). These properties are attractive for many industries like anti-biofouling paints for boats, anti-sticking of snow for antennas and windows, lab-on-chip device and so on (Subhash Latthe et al., 2012).

Artificial superhydrophobic surfaces are produced employing two kinds of approaches: create hierarchical structures (micro- and nanostructures) on hydrophobic substrates, or to chemically modify a hierarchical structured surface with a low surface free energy material (Figure 12) (Guo et al., 2011).

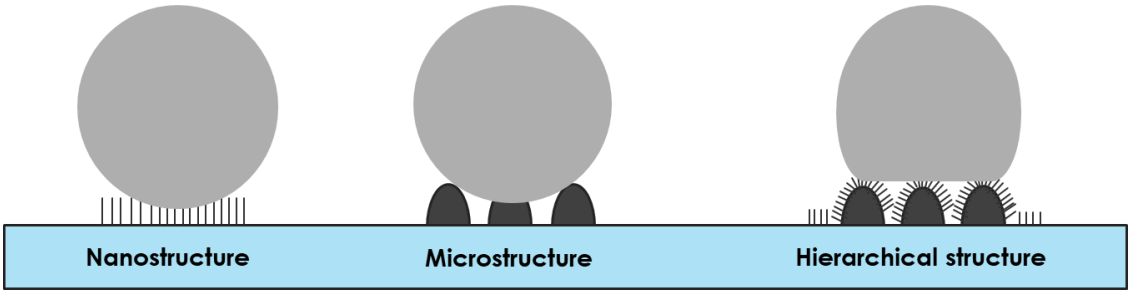

Figure 12 Structural representation of artificial superhydrophobic surfaces. Adapted from Nosonovsky and Bhushan (2009)

Currently, there are several methods to fabricate superhydrophobic surfaces. These methods can be categorized in two ways: "top-down" and "bottom-up" approaches (Li et al., 2007). A top-down approach refers to a generation of superhydrophobic nanoscale functional devices with the preferred shapes and characteristics, starting on a larger scale, where the surface nanotopography required for the condition on superhydrophobicity was imparted through the removal of the material. Bottom-up approaches, conversely, tend to employ construction approaches whereby the topographical conditions for superhydrophobicity are achieved through nanoscale assembly of structures based on intricate techniques and systems (Crawford et al., 2015; Li et al., 2007).

There are also methods based on the combination of both approaches, for example, electrospinning (Papadopoulou et al., 2011) and phase separation (Song et al., 2010). Table 9 summarizes some of the methods used to fabricate artificial superhydrophobic surfaces, as found in some reference works.

Table 9 Methods to produce artificial superhydrophobic surfaces.

Method		**Description**	**References**
Top –down approaches	Templating	In this technique, a suitable 2D or 3D pattern is filled with a soft material, and then the material is hardened. The template is posteriorly removed by a suitable method, keeping the replica intact.	(Roach et al., 2008)
	Lithography	The light is irradiated through a mask with the desired features on subtracts, with a photoresist. Subsequent etching steps yield the desired pattern surfaces.	(Li et al., 2007)
Bottom-up approaches	Chemical Vapour deposition	This method utilizes a mixture of chemically reactive components, which are deposited on the surface, leaving the desired thin layer of coating.	(Puliyalil et al., 2015)
	Sol-gel	A sol is prepared by hydrolysis and polycondensation of the corresponding oxide in the presence of the solvent. During the network formation, a large amount of solvent is also impregnated in the network and thus a gel is formed.	(Li et al., 2007)
Bottom-up and top-down combination	Phase separation	A polystyrene (PS) solution in tetrahydrofuran is prepared and mixed with ethanol. The mixture is dispersed in a smooth PS commercial substrate, which is immersed in ethanol and dried with a nitrogen flow. To increase the superhydrophobicity, the rough PS surfaces are modified with PFDTS[1] after an argon plasma treatment.	(Lima et al., 2011)

[1] Perfluorodecyltriethoxysilane

Microencapsulation based on superhydrophobic surfaces has gained a considerable interest in the scientific community. According to Song et al. (2010), this method can be pottentionaly applied in tissue engineering or as a support for cell expansion, cell

encapsulation and as spherical structures for controlled release of molecules. Potential advantages of this method include (Lima et al., 2013; Song et al., 2010):

i) Individual solification of spherical hydrogel in a dry environment at room temperature;
ii) Easy operation for preparing hydrogel spheres;
iii) High encapsulation efficiency and high encapsulation loading of cells;
iv) Production of almost shperical hydrogel particles without mechanical stress, stirring, use of organic solvents, high temperature and pressures;
v) Low cost production costs and scale-up possibility using a friendly technology;

Due to the described advantages, superhydrophobic surfaces started to be viewed as interesting alternatives to support microencapsulation techniques. This interest generated already the development of several works where this technique was explored. The examples include the use of systems with chitosan, dextran, and also alginate (Lima et al., 2013).

Song et al., (2010) described a fabrication process of alginate microspheres using a polystyrene superhydrophobic surface prepared by a phase separation process. Firtsly, the behaviour of alginate microshperes cointainig teophyline as active agent was analyzed. The alginate droplets were crosslinked *in situ* after addition of small volumes of calcium chloride on the top side of the droplets. It was observed that, for 2% and 3% alginate solutions, there was a 100% efficiency of drug release. In a second study, they analyzed alginate microspheres containing L929 cells. The obtained shperes had a regular shape, with a diametter of 3mm approximatelly. The behaviour of chitosan microspheres, crooslinked with genipin, containing Fe_3O_4 magnetite particles was also analyzed in this work. The resulted microspheres showed particles with a strong density of irregular pores and sizes up to 10µm.

Puga et al., (2013) used superhydrophobic surfaces to produce chitosan microgels using 5-fluorouracil (antitumoral drug) as an active principle. Droplets of drug-contained chitosan aqueous solution were dispersed in a polystyrene superhydrophobic surface. The droplets were crosslinked in a glutaraldehyde atmosphere and coated with a drug-free chitosan or pectin. The results showed that the microgels had an encapsulation efficiency of 100%, with diameters in the range between 200µm and 600µm.

Lima et al., (2011) also used this methodology to produce smart hydrogel beads composed by a photo-crosslinked dextran-methacrylated and thermal responsive poly(N-isopropylacrylamide) mixed with a protein (insulin or albumin), in several superhydrophobic surfaces (polystyrene, cupper and alluminium). The spheres were hardened in a dry environment under UV light. The results showed that the shperical hydrogel particles were formed in a few minutes, with almost 100% encapsulation yield.

Table 10 shows some works using superhydrophobic subtrates, as well their fabrication process, to produce polymeric spheres and their main applications.

Table 10 Reported works using superhydrophobic substrates to produce microspheres.

Active Principle	**Encapsulation Material**	**Surface/ Treatment**	**Apllication**	**References**
5-Fluororacil	Chitosan	Polystyrene (Argon Plasma Treatment)	Oral and Topical Chemotherapy	(Puga et al., 2013)
Teophypline	Chitosan	Polystyrene (Phase inversion)	Support for cell expansion, Cell Encapsulation or Spherical structures for controlled release of molecules	(Song et al., 2010)
E.coli (cells)	PTFE[2] incorporated in curable PMDS[3]	Silicon Wafer (Spin coating)	Implantable microelectronics devices	(Xiu et al., 2006)
Dexamethasone and L929 Cells	Chitosan	Polystyrene (Phase Separation)	Drug Delivery	(Lima et al., 2014)
Mesenchymal stem cells	Alginate	Polystyrene (Phase separation)	Bone Regeneration	(Lima et al., 2013)

2 Polytetrafluoroethylene; 3 Polydimethylsiloxane

3.Materials and Methods

3.1 Standards and Reagents

Calcium chloride di-hydrate and Tween 80® were purchased on Pancreac Applichem, Sodium Alginate was purchased at Fluka Chemika, Safranin O was purchased on Merck, Curcumin (≥94 %), Calcium D-gluconate monohydrate (≥98%), Calcium L-lactate hydrate were purchased at Sigma-Aldrich. Ethanol (≥99.8%) was purchased to Honeywell, Riedel-de Haën. The polystyrene (PS) superhydrophobic surfaces were kindly provided by Professor João Mano, from Universidade de Aveiro.

3.2 Methods

3.2.1 Curcumin Suspension

Once curcumin is a hydrophobic compound, its encapsulation by using alginate comprises an initial stage where curcumin suspension in water is prepared. For this purpose, 20 ml of distillate water were added to a beaker together with 100 mg of curcumin (0.5% w/v) and 100 µl of emulsifier (Tween 80®). Then, the mixture was homogenized for 20 minutes by using a CAT Unidrive X homogenizer at 11000 rpm. Afterwards, 800 mg of sodium alginate (4% (w/v), curcumin/alginate ratio: 0.125) were added to the suspension which were kept under stirring until the alginate dissolution was completed.

3.2.2 Safranin solution

Safranin solution was prepared by dissolving 100 mg of safranin (0.5 % w/v) in 20 ml of distillate water. After the complete dissolution of safranin, 800 mg of alginate (4% (w/v), safranin/alginate ratio: 0.125) were added to this solution, being further kept under stirring until the full dissolution of alginate was achieved.

3.2.3 Spray-coagulation Method

This section describes the procedure for the microspheres (MIC) production by using the spray-coagulation process, being the followed procedure according to the work of Rached et al. (2016). The process started with the preparation of the coagulation solution, with concentration of 4% (w/v), being the total used volume of 250 ml for each ionic crosslinker tested ($CaCl_2$, Ca-Glu, Ca-Lact, 4% (w/v)). The emulsion or solution, depending on the used active principle, curcumin or safranin, prepared according to the

procedure previously stated, was introduced into a syringe and placed on the syringe pump of the atomization system (Figure 13). The flow rate of the solution addition and the pressure of the atomizing gas were established in 0.3 ml/min and 0.1 bar, respectively. The distance between the nozzle and the coagulation solution was 7 cm. For each assay, the volume of the emulsion/solution atomized was 7.0 ml. At the end of the atomization process, the coagulation solution was kept under stirring during 4 hours at room temperature, in order to promote the MIC gelation/crosslinking. After 4 hours, the MIC were recovered by filtration and washed twice with distillate water. Next, the MIC were freeze-dried and stored at 4ºC for further studies.

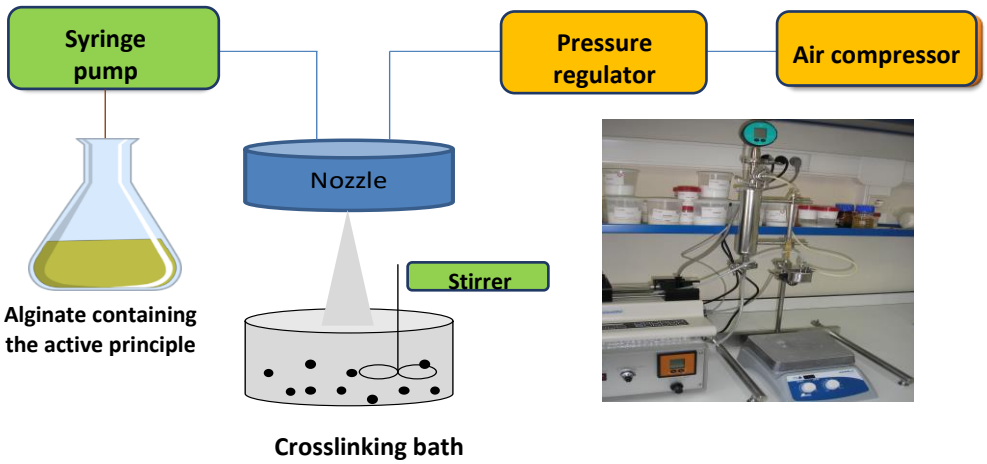

Figure 13 Schematic representation of the atomization system (Nisco Var J30) (Viegas et al., 2013).

3.2.4 Superhydrophobic Surface Method

The production of MIC using superhydrophobic surfaces was based in the work of Lima et al. (2013). This process started with the preparation of the coagulation solution ($CaCl_2$, Ca-Glu, Ca-Lact, 4% w/v). Then, after preparing the alginate/safranin solution or the alginate/curcumin suspension, the MIC were produced by putting the suspension or solution drops (5µl) on the PS superhydrophobic surface, by using a micropipette. After, 2µl of the coagulation solution were added on the top of each droplet to promote the alginate gelation/crosslinking, which was allowed to occur for 1 hour. The MIC formation and gelation was monitored by optical microscopy, in order to analyze their morphology and behavior throughout the process. Figure 14 presents a schematic representation of the microencapsulation process using the SH surface.

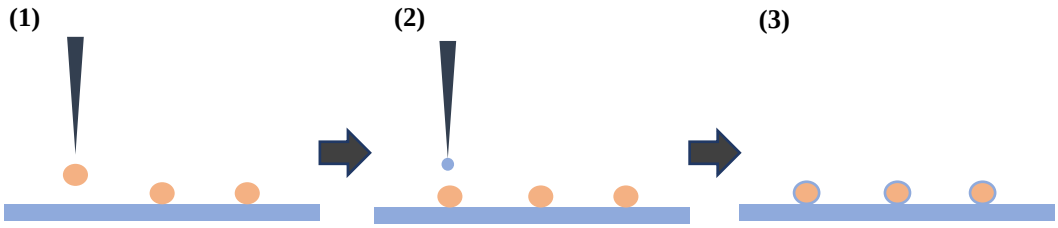

Figure 14 Schematic process of microencapsulation using SH surface.

3.3 Microspheres Characterization

3.3.1 Optical Microscopy

The morphology of the produced MIC was analyzed by using the optical microscope Ni-U (Nikon Eclipse*i*) equipped with a digital camera and a NIS-Elements Documentation software. The images were acquired with magnifications of 40x, 100x, 200x and 400x.

3.3.2 Calibration curves built-up

The quantification of the active principle was done based on a calibration curve prepared from standard solutions. The wavelength used to measure the absorbance was determined by a preliminary scan through all the visible spectra region by using a spectrophotometer (Jasco V530 UV/vis, Japan). The maximum absorption wavelength was registered at 420 nm for curcumin and 517 nm for safranin. Afterwards, the calibration curves (Abs= 161315.C – 0.0503 (R^2=0.993) for curcumin and Abs=144013.C – 0.3225 (R^2=0.996) for safranin) were obtained by using 5 standard solutions, with concentrations between 0,033 mg/mL and 6,66x10^{-3} mg/mL for curcumin and between 0,034 mg/ml and 6,68x10^{-3} mg/mL for safranin, being these values based on the maximum amount of encapsulated active principle.

3.3.3 Encapsulation Efficiency

The evaluation of the encapsulation efficiency (EE) was based on the quantification of the amount of active principle effectively encapsulated. The EE was calculated by establishing the ratio between the amount of encapsulated active principle and the theoretical amount (M_{theo}), according to the equation (1). The amount of encapsulated active principle is calculated by the difference between the theoretical amount (M_{theo}) and the non-encapsulated active principle ($M_{n.enc.}$). The non-encapsulated corresponds to the

amount lost during the coagulation staged. So, in order to quantify the amount lost, the coagulation solution was recovered by filtration and analyzed in UV-vis (Jasco V-530 spectrophotometer, at λ=420 nm for curcumin and λ= 517 nm for safranin), in order to evaluate the mass of each one present.

$$EE\ (\%) = \frac{M_{theo} - M_{n.enc.}}{M_{theo}} \times 100 \qquad \text{Eq. (1)}$$

3.3.4 Load

The load concept is used to express the amount of active principle encapsulated in the produced MIC. This parameter was calculated by using equation (2):

$$Load\ (w/w) = \frac{M_{theo}}{M_{ds}} \times EE \qquad \text{Eq. (2)}$$

Where M_{theo} corresponds to the theoretical amount of active principle and M_{ds} corresponds to the weight of dried substances ($M_{Alginate} + M_{theo}$).

3.3.5 Dry Residue

The dry residue corresponds to the weight of MIC obtained after the water removal. It was determined by the ratio between the weight of dry MIC (after freeze drying) and the weight of hydrated MIC (after the crosslinking stage), expressed as a percentage (% w/w).

3.3.6 Rehydration capacity

The rehydration capacity is related with the ability of the MIC to adsorb water and recover the initial shape. This evaluation was carried out by putting 30 mg of freeze-dried MIC, crosslinked with the different calcium sources, into 10 ml of distilled water. The samples were stored during 72h. After this time-period, the MIC were analyzed by optical microscopy to access the morphology, being after weighted to evaluate the weight gain. This parameter was calculated using equation (3):

$$R.C = 1 - \left(\frac{M_{hum} - M_{reh}}{M_{hum}}\right) \times 100 \qquad \text{Eq. (3)}$$

Where M_{hum} corresponds to the weight of humid MIC (after production) and M_{reh} refers to the MIC weight after rehydration.

3.3.7 Release profile

Having in view the study of the active principle (curcumin or safranin) release mechanism, the release profile of the freeze-dried MIC was evaluated. Due to the hydrophobic nature of curcumin, its release profile was study by using two different solvents: distilled water and ethanol. For safranin, due to its hydrophilicity only water was used as solvent.

The release profile was evaluated according to the following procedure:

1. 30 mg of dry MIC were weighed;
2. The MIC were placed on 10 ml of solvent;
3. After, 4 ml of the supernatant was removed, and the absorbance was measured in a UV-vis spectrophotometer. The supernatant solution was placed again in the respective vial and the procedure was repeated hourly during the first 8 hours and then every 24 hours until a total period of 72 hours was complete.

The quantification of the active principle amount was done based on the calibration curves previously built.

3.3.8 Fourier Transform Infrared Spectroscopy

FTIR spectra were obtained on ABB Inc. FTIR, model MB3000 (Quebec, Canada) in transmittance mode by using KBr pellets with a sample concentration of 1% (w/w). Spectra were recorded between 550 and 4000 cm^{-1} at a resolution of 16 cm^{-1} and a cumulative of 32 scans. Spectra were acquired and treated (baseline correction) using the software Horizon MB v.3.4.

3.3.9 Particles size characterization

The freeze-dried MIC were analyzed in a laser diffraction equipment Malvern Mastersizer 3000, equipped with a dispersion unity Hydro MV (Malver, United Kingdom). Distilled water was used as solvent to disperse the dried microspheres and the

analysis were made by using 5 measurements for each sample, which allowed to determine the volume and number distributions of the samples.

3.3.10 Thermal Properties

The thermogravimetric analysis (TGA) were made using a NETZSCH model TG 209F3 Tarsus (Selb, Germany) equipment. Approximately 6-7 mg of the obtained MIC were heated in alumina crucibles from 32 until 900ºC in a constant heating rate of $10^{o}C.min^{-1}$. The experiments were made under nitrogen flow (50 mL/min). Thermograms were treated with Netzsch Proteus- thermal analysis software, version 5.2.1.

4.Results and Discussion

4.1 Microencapsulation of hydrophobic and hydrophilic active principles using the spray-coagulation method

The present work has as main objective the microencapsulation of hydrophobic and hydrophilic active principles, namely curcumin and safranin, using alginate as matrix and different calcium salts as ionic crosslinkers, by the spray/coagulation method. For comparison purposes, empty MICs (without active principle) were also produced for all the chemical systems. The samples were named according to the active principle and the crosslinker used, so "Mic_Alg_$CaCl_2$, Ca-Glu or Ca-Lact" means "Empty alginate microspheres crosslinked with $CaCl_2$, Ca-Glu or Ca-Lact", respectively, while "Mic_Curc_$CaCl_2$, Ca-Glu or Ca-Lact" means "Curcumin microspheres crosslinked with $CaCl_2$, Ca-Glu or Ca-Lact", respectively and "Mic_Safr_ $CaCl_2$, Ca-Glu or Ca-Lact" means "Safranin microspheres crosslinked with $CaCl_2$, Ca-Glu or Ca-Lact". Tables 11, 12 and 13 summarizes the production conditions and the weight of the obtained MIC after the production. Two assays were performed for each active principle, in order to recover an enough amount of MIC to perform all the subsequent studies. So, the values from tables 12, 13, 14, 15, 17 and 18 are expressed as mean values of the two assays. The obtained values for each assay can be consulted in Appendix A.

Table 11 Production of empty alginate microspheres crosslinked with different calcium sources.

Sample	Atomized volume (ml)	Weight of wet MIC (mg)
Mic_Alg _$CaCl_2$	13	2623.7
Mic_Alg_Ca-glu	13	2520.7
Mic_Alg_Ca-lact	13	2458.7

Table 12 Production of curcumin MIC crosslinked with different calcium sources.

Sample	Atomized volume (ml)	Weight of wet MIC (mg)
Mic_Curc_$CaCl_2$	7	922.35±0.05
Mic_Curc_Ca-glu	7	965.6±0.04
Mic_Curc_Ca-lact	7	967.25±0.02

Table 13 Production of safranin MIC crosslinked with different calcium sources.

Sample	Atomized volume (ml)	Weight of wet MIC (mg)
Mic_Safr_$CaCl_2$	7	1075.35±0.06
Mic_Safr_Ca-glu	7	1202.45±0.09
Mic_Safr_Ca-lact	7	1048.51±0.07

4.1.1 Optical Microscopy

Figure 15, 16 and 17 shows OM images acquired with magnifications of 40, 100, 200x and 400x or the empty MIC, curcumin and safranin MIC, respectively, at the end of the coagulation stage and according to the different used coagulation solutions.

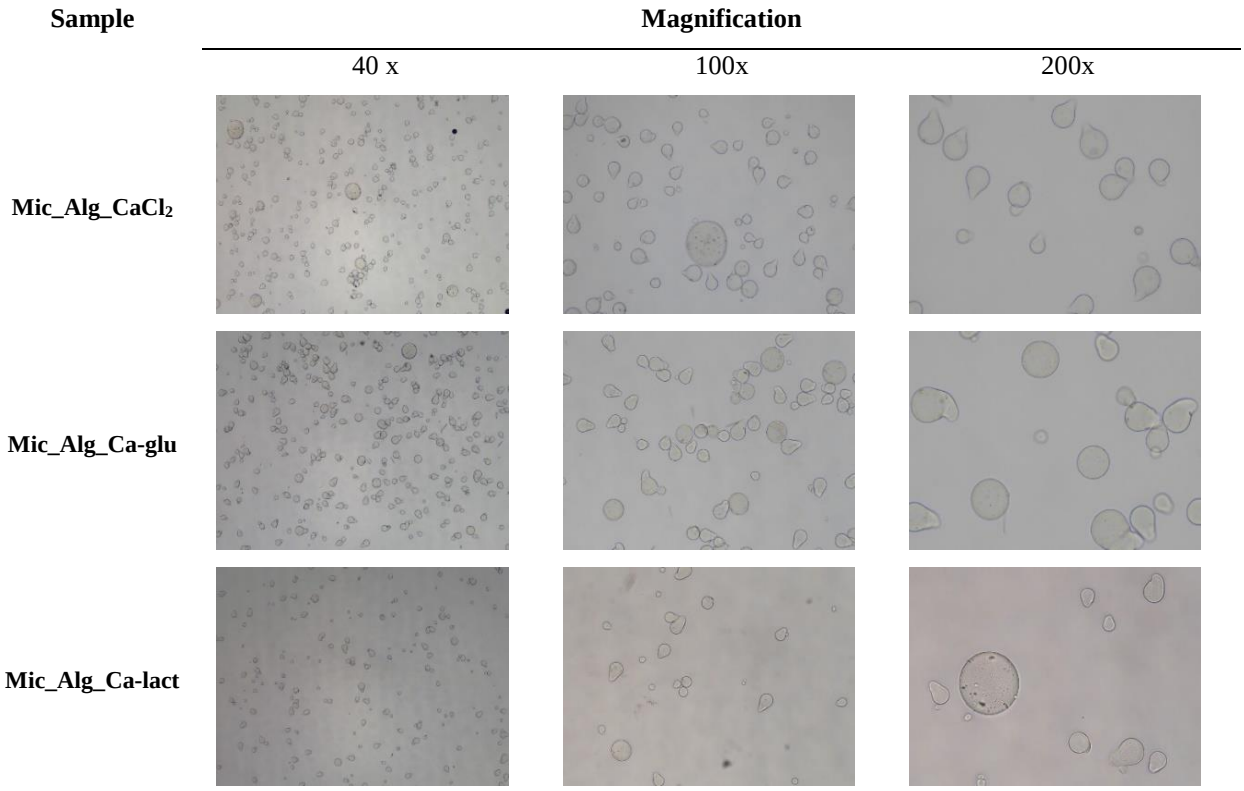

Figure 15 Empty alginate MIC morphology after the coagulation step (time of 4h).

Sample	Magnification		
	40 x	200 x	400x
Mic_Curc_$CaCl_2$	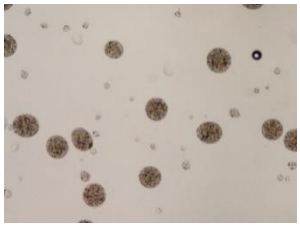	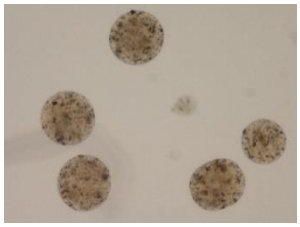	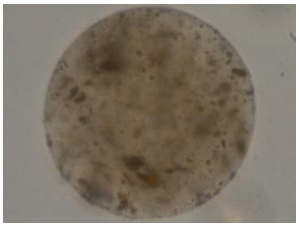
Mic_Curc_Ca-glu	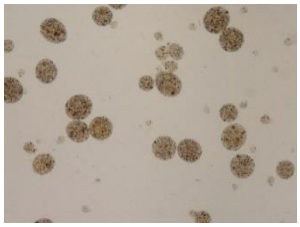	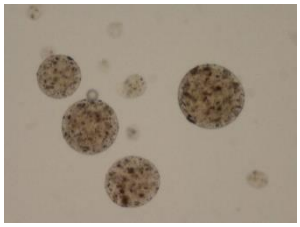	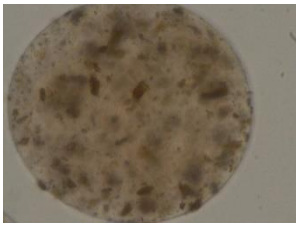
Mic_Curc_Ca-lact	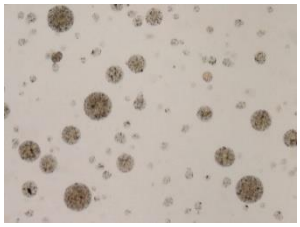	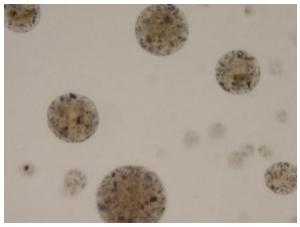	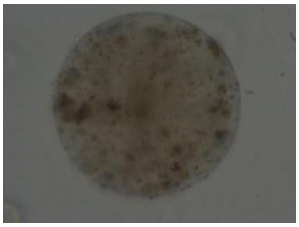

Figure 16 Curcumin's MIC morphology after the coagulation step (time of 4h).

Sample	Magnification		
	40 x	100x	200x
Mic_Safr_ $CaCl_2$	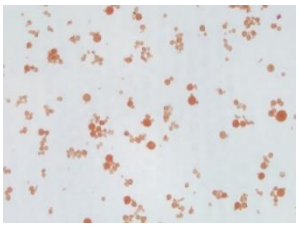	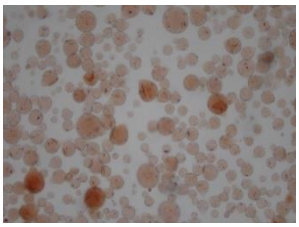	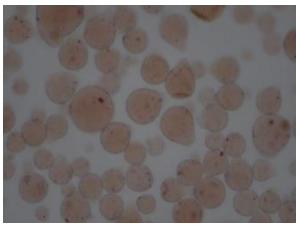
Mic_Safr_Ca-glu	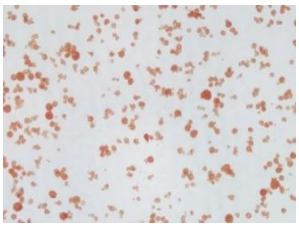	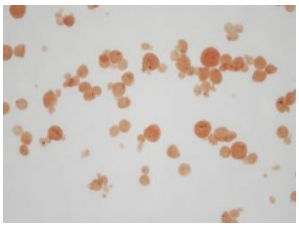	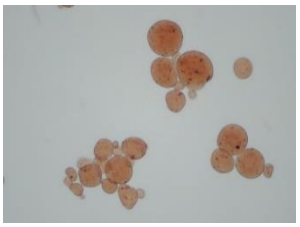
Mic_Safr_Ca-lact	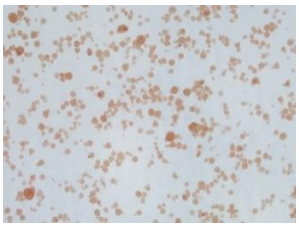	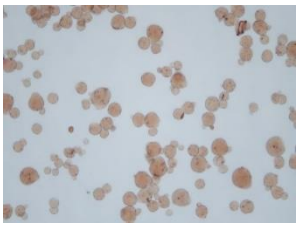	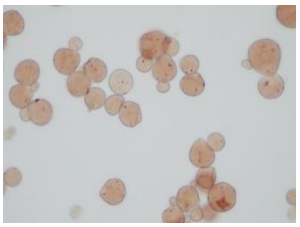

Figure 17 Safranin's MIC morphology after the coagulation step (time of 4h).

Analyzing the obtained images, the following features can be noticed:

- After the coagulation period of 4 hours, for the empty MIC (Figure 15), a spherical conformation can be noticed. However, a predominance of a pear shape is detected mainly for the MIC produced with $CaCl_2$ and Ca-glu;
- The curcumin MIC (Figure 16) have a spherical conformation, and it is possible to observe the presence of small curcumin crystals on the surface;
- For safranin MIC (Figure 17), a predominant spherical conformation can be identified. However, the presence of microspheres with some deformation are also detected, especially for the MIC produced with $CaCl_2$.

Considering the different calcium sources used, it can also be seen that the Ca-glu crosslinked MIC presented some agglomeration after coagulation, whereas the $CaCl_2$ and Ca-lact crosslinked MIC became more dispersed. Figure 18, 19 and 20 presents the analysis by OM of the produced MIC after freeze drying.

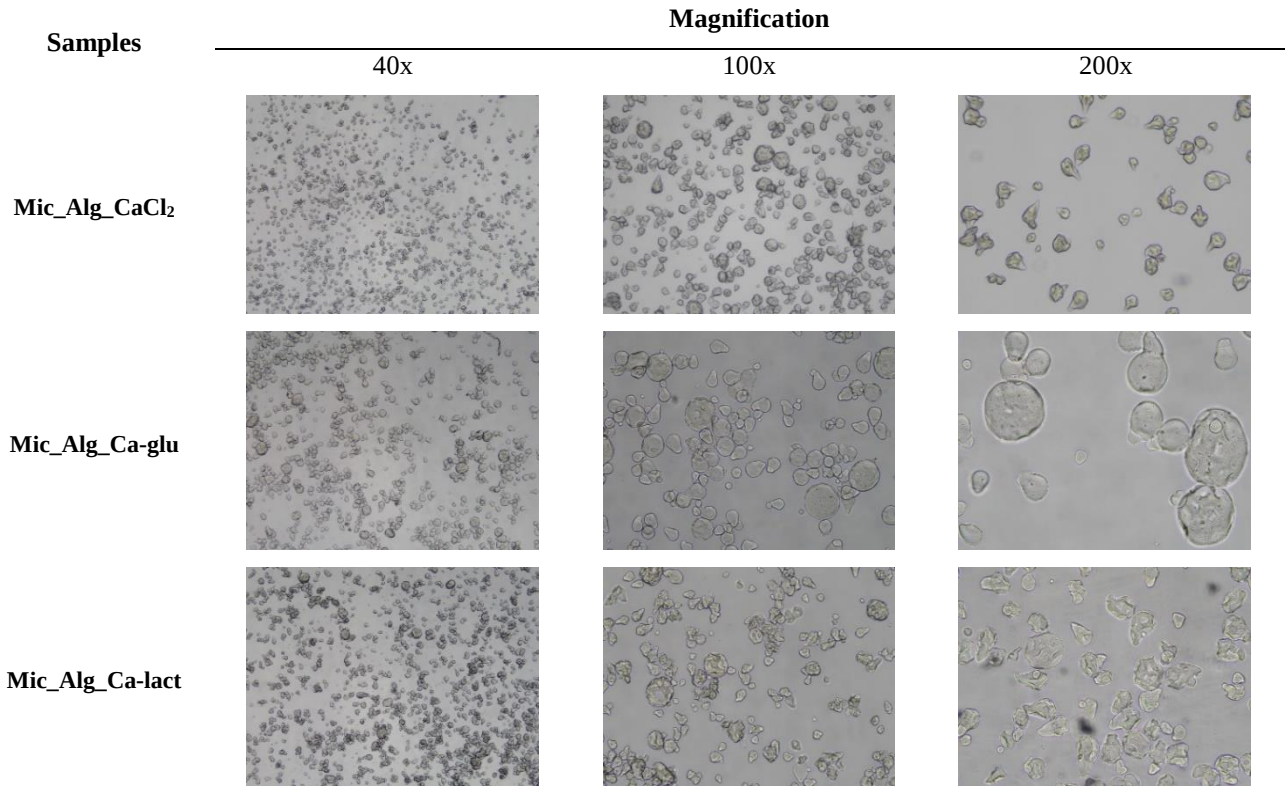

Figure 18 Empty alginate MIC morphology after the freeze drying.

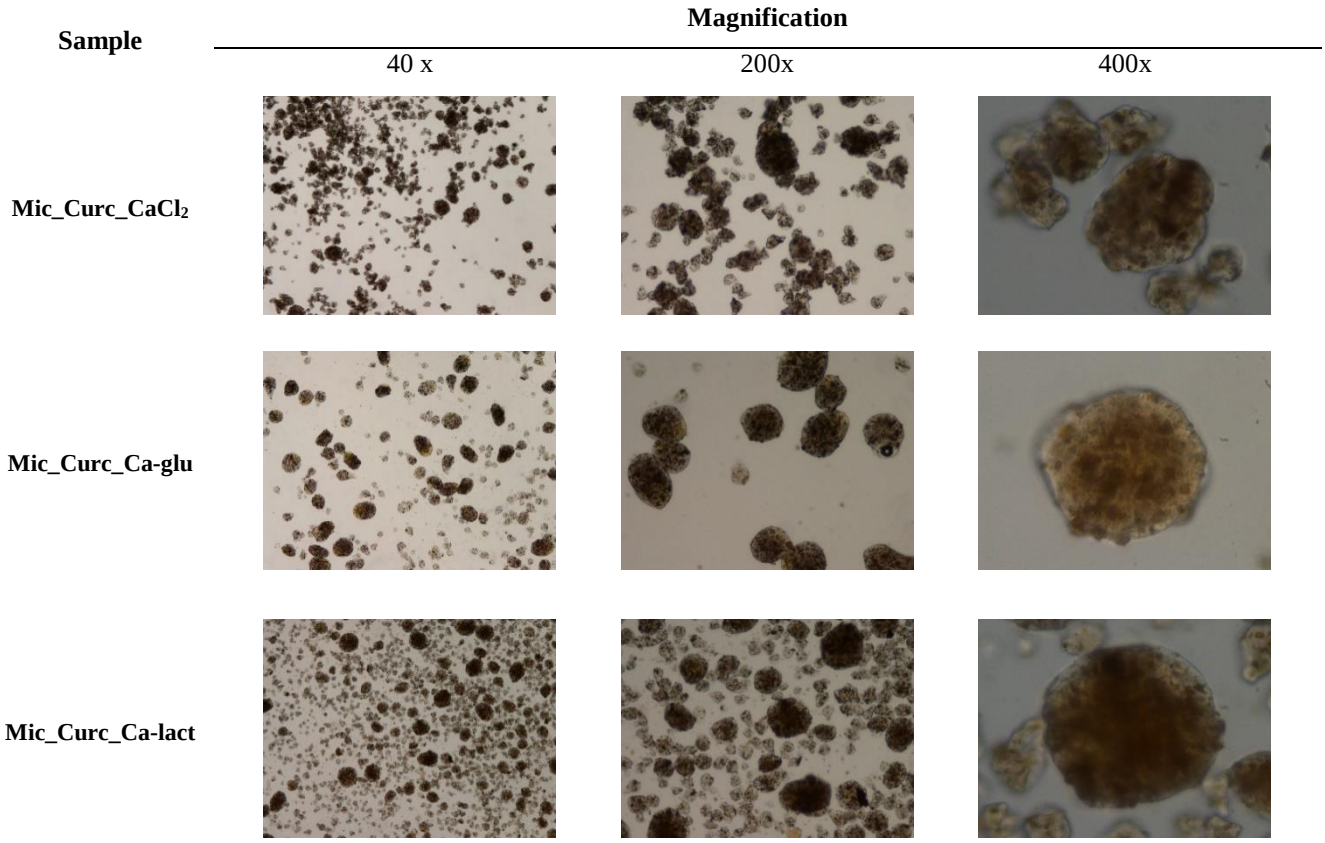

Figure 19 Curcumin MIC morphology after the freeze drying.

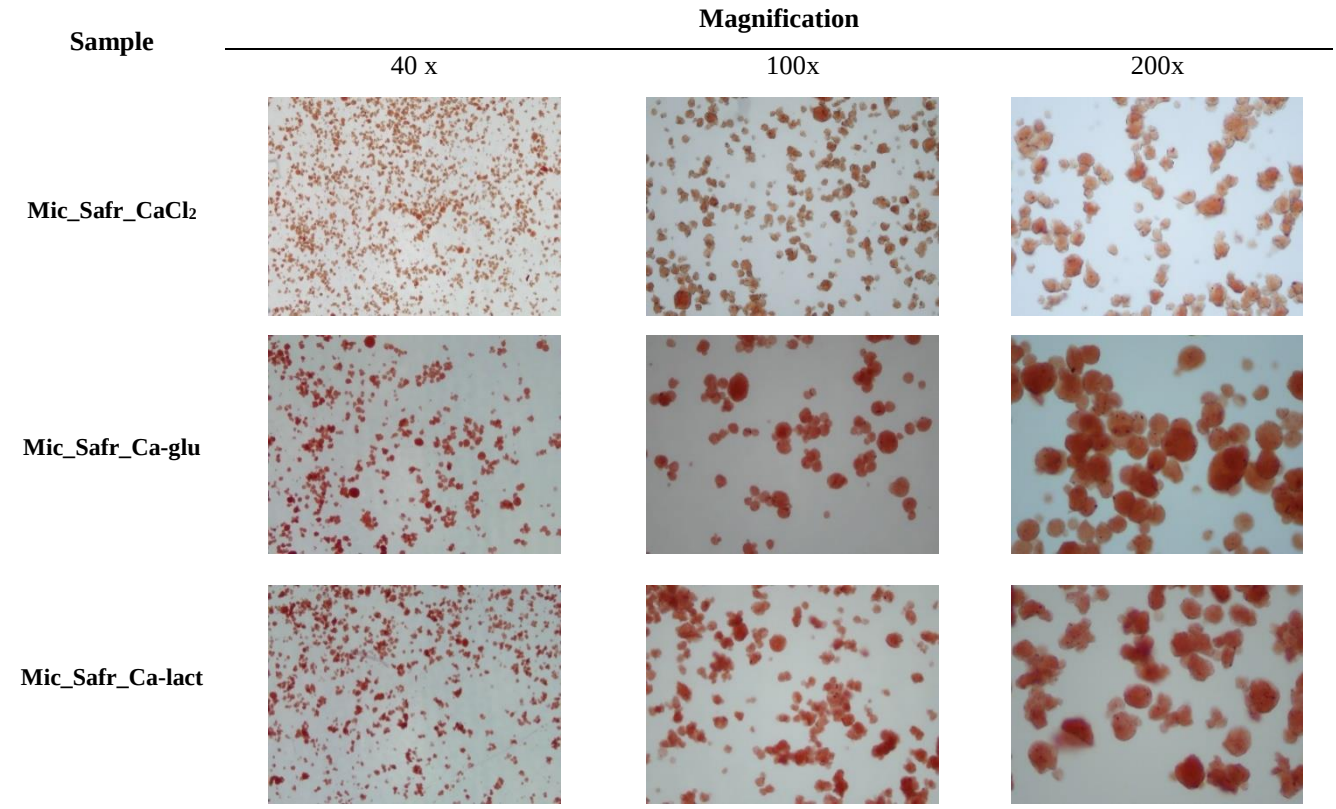

Figure 20 Safranin's MIC morphology after the freeze drying.

After the freeze-drying process, it can be observed that the empty MIC had lost the initial shape due to the water lost. The curcumin MIC were also deformed due to the water removal. Regarding the safranin ones, a higher deformation is evidenced, comparatively with the curcumin MIC.

4.1.2 Encapsulation Efficiency and load

The encapsulation efficiency (EE, %) is a variable that allows the quantification of the amount of active principle encapsulated and can be achieved by analyzing the amount that has not been encapsulated or lost during the microparticles consolidation stage. The quantification was done by UV-vis. Table 14 and 15 presents a mean value for the encapsulation efficiency (% w/w) and load (w/w), for curcumin and safranin MIC respectively, using the three different crosslinking agents.

Table 14 Encapsulation efficiency and load for the curcumin MIC.

Curcumin		
Sample	**EE (%, (w/w))**	**Load (w/w)**
Mic_Curc_$CaCl_2$	99.25±0.15	0.1103
Mic_Curc_Ca-glu	98.45±0.25	0.1095
Mic_Curc_Ca-lact	97.91±0.30	0.1087

Table 15 Encapsulation efficiency and load for the safranin MIC

Safranin		
Sample	**EE (%, (w/w))**	**Load (w/w)**
Mic_Safr_$CaCl_2$	98.51±0.18	0.1095
Mic_Safr_Ca-glu	97.95±0.05	0.1089
Mic_Safr_Ca-lact	97.42±0.06	0.1083

Analyzing the results presented in table 14 and 15, it can be noticed that all the samples present high values for the encapsulation efficiency. For curcumin, due to its hydrophobicity it wouldn't be expected a significant loss for the crosslinking aqueous

solution, during the coagulation stage. The mean EE values were 99.25%, 98.45% and 97.91%, respectively for the MIC crosslinked with $CaCl_2$, Ca-glu and Ca-lact.

Regarding the safranin MIC, high EE values were also obtained. This was not expected, once safranin is a hydrophilic compound with good chemical compatibility with the coagulation aqueous solution, being thus expected a great loss during the coagulation stage. The values of EE obtained varied from 98.51% for the $CaCl_2$ MIC to 97.95% for the Ca-glu MIC and 97.42% for the Ca-lact MIC.

Analyzing the EE values obtained on this study from the perspective of the used crosslinkers influence, an effect of the calcium dissociation constant values (pKa) can be foresee. According to Schaller (2008), the lower the dissociation constant value (including negative values), the greater is the dissociation capacity of the compound. So, $CaCl_2$ dissociates faster than the other crosslinkers (pKa = -7), being followed by Ca-glu (pKa = 3.70) and, finally, Ca-lact (3.78). The contact of the alginate droplets with the crosslinking solution results in an immediate superficial coating formation. This coating limits the active principle diffusion for the coagulation solution, increasing consequently, the EE. In this sense, since $CaCl_2$ has a faster dissociation, higher EE values are expected when this crosslinker is used. Beyond these considerations, other factors that can be related with these values is the calcium ions content in the crosslinking solutions. By analyzing the molar balance between the G alginate groups and the Ca^{2+} present in the three crosslinking solutions, it was noticed that $CaCl_2$ solution has an excess of Ca^{2+} 45-fold higher than the required for the alginate crosslinking, being followed by Ca-lact solution with 25-fold and by Ca-glu where an excess of 11-fold was used.

4.1.3 Dry Residue

Table 16, 17 and 18 shows the dry residues values (%w/w) calculated for the empty microspheres, curcumin and safranin ones respectively, crosslinked with the three different calcium sources.

Table 16 Production of empty alginate microspheres crosslinked with different calcium sources.

Sample	Weight of wet MIC (mg)	Weight of dry MIC (mg)	Dry Residue % (w/w)
Mic_Alg _$CaCl_2$	2623.7	153.6	5.9
Mic_Alg_Ca-glu	2520.7	165.2	6.6
Mic_Alg_Ca-lact	2458.7	139.5	5.7

Table 17 Production of curcumin MIC crosslinked with different calcium sources.

Sample	Weight of wet MIC (mg)	Weight of dry MIC (mg)	Dry Residue % (w/w)
Mic_Curc_$CaCl_2$	922.4	80.2	8.7±1.55
Mic_Curc_Ca-glu	965.6	97.8	10.2±0.92
Mic_Curc_Ca-lact	967.3	95.8	9.86±1.86

Table 18 Production of safranin MIC crosslinked with different calcium sources.

Sample	Weight of wet MIC (mg)	Weight of dry MIC (mg)	Dry Residue % (w/w)
Mic_Safr_$CaCl_2$	1075.4	102.4	9.5±0.21
Mic_Safr_Ca-glu	1202.5	115.1	11.2±0.45
Mic_Safr_Ca-lact	1048.5	106.3	10.2±0.5

Based on the weight measured after freeze drying, a dry residue of 5.85 % was obtained for the empty MIC crosslinked with $CaCl_2$, 6.55% for the ones with Ca-glu and 5.67% for the ones with Ca-lact. The values obtained for the dry residue for the curcumin MIC were 8.61% for the $CaCl_2$ crosslinked MIC, 10.17% for the Ca-glu ones and 9.86% for the Ca-lact. Regarding the safranin MIC, the dry residue was 9.49%, 11.13% and 10.17%, respectively for the $CaCl_2$, Ca-glu and Ca-lact crosslinked MIC.

4.1.4 Rehydration Capacity

For this test, the freeze-dried MIC were rehydrated in distilled water, in order to evaluate the ability to recover their initial shape. Tables 19, 20 and 21 shows the weight of the samples before and after the test, as well the rehydration capacity value (% w/w).

Table 19 Rehydration capacity results for the empty microspheres.

Sample	MIC Initial weight t=0 (mg)	Correspondent weight of humid MIC (mg)	MIC Final weight t=72h (mg)	Rehydration capacity (% w/w)
Mic_Alg_$CaCl_2$	30	512.4	61.7	12.1
Mic_Alg_Ca-glu	30	457.8	181.1	39.6
Mic_Alg_Ca-lact	30	529.2	82.1	15.5

Table 20 Rehydration capacity results for the curcumin microspheres.

Sample	MIC Initial weight t=0 (mg)	Correspondent weight of humid MIC (mg)	MIC Final weight t=72h (mg)	Rehydration capacity (% w/w)
Mic_Curc_$CaCl_2$	30	424.7	48.9	11.5
Mic_Curc_Ca-glu	30	324.4	77.1	23.7
Mic_Curc_Ca-lact	30	375.0	57.9	15.2

Table 21 Rehydration capacity results for the safranin microspheres.

Sample	MIC Initial weight t=0 (mg)	Correspondent weight of humid MIC (mg)	MIC Final weight t=72h (mg)	Rehydration capacity (% w/w)
Mic_Safr_$CaCl_2$	30	308.9	56.1	18.2
Mic_Safr_Ca-glu	30	298.8	128.3	42.9
Mic_Safr_Ca-lact	30	301.4	98.2	32.6

Analyzing the results described in tables 19, 20 and 21 it can be observed that the Ca-glu crosslinked MIC, in all the cases, have a good rehydration capacity, followed by the Ca-lact crosslinked MIC and, finally, the $CaCl_2$ MIC. Figure 21, 22 and 23 shows the microspheres OM images after the rehydration test. It is worth to mention that no studies were found about the crosslinkers molecular structure effect on the MIC morphology. The only study found is focused on the rate of alginate consolidation by using the three calcium sources (Lee and Rogers, 2012).

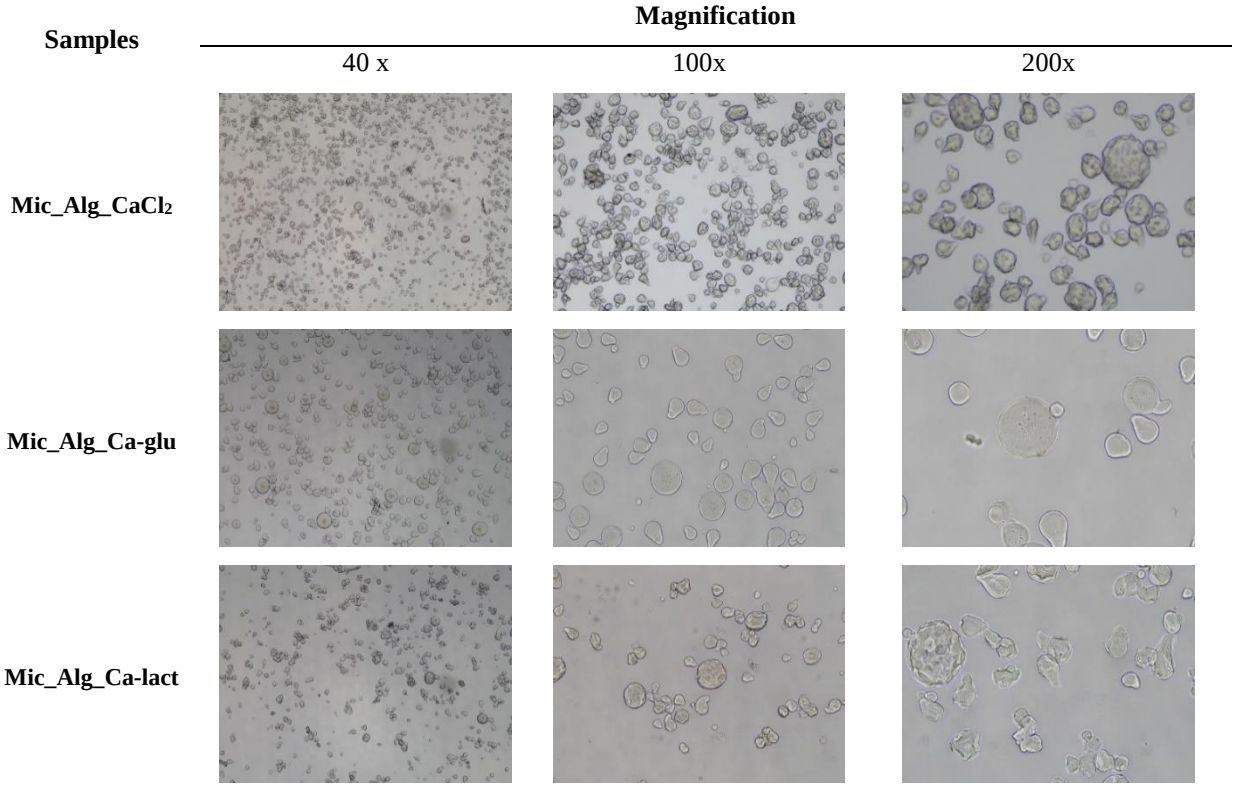

Figure 21 Alginate MIC morphology after the rehydration capacity test.

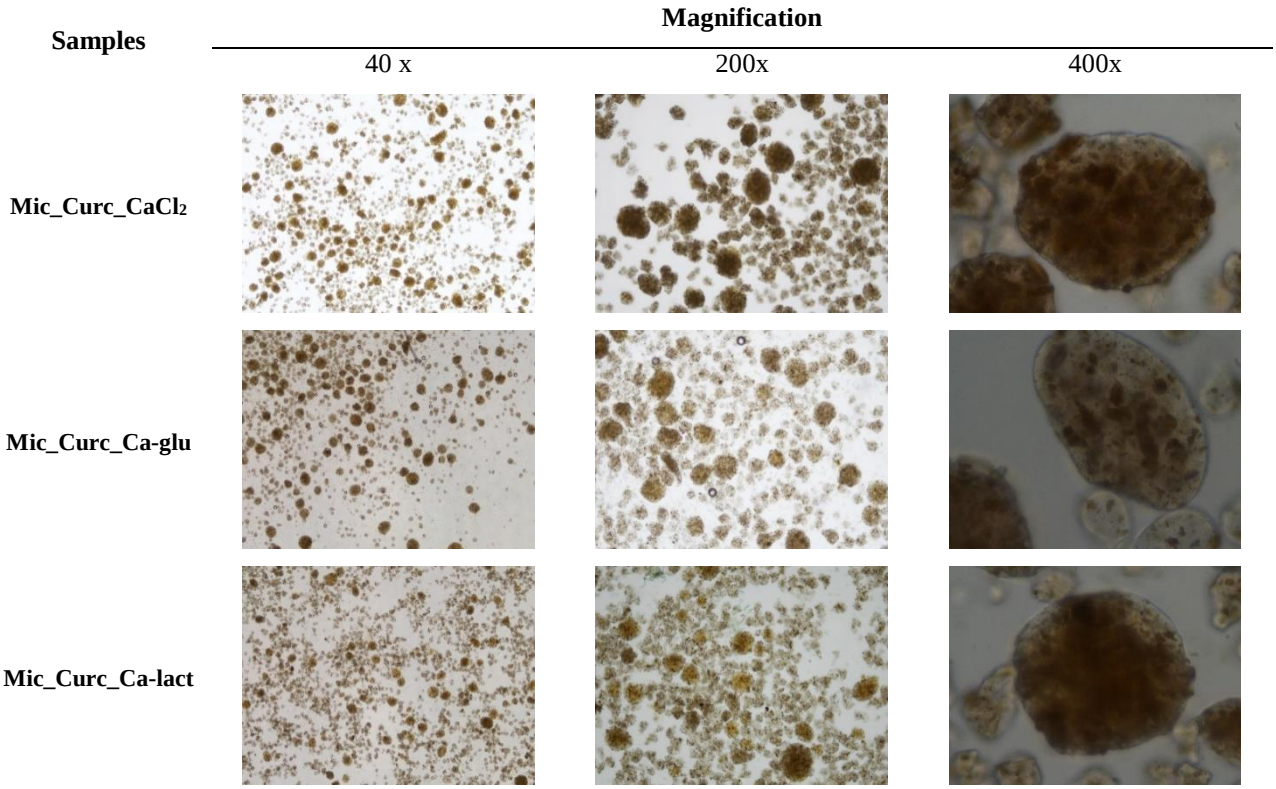

Figure 22 Curcumin's MIC morphology after the rehydration capacity test.

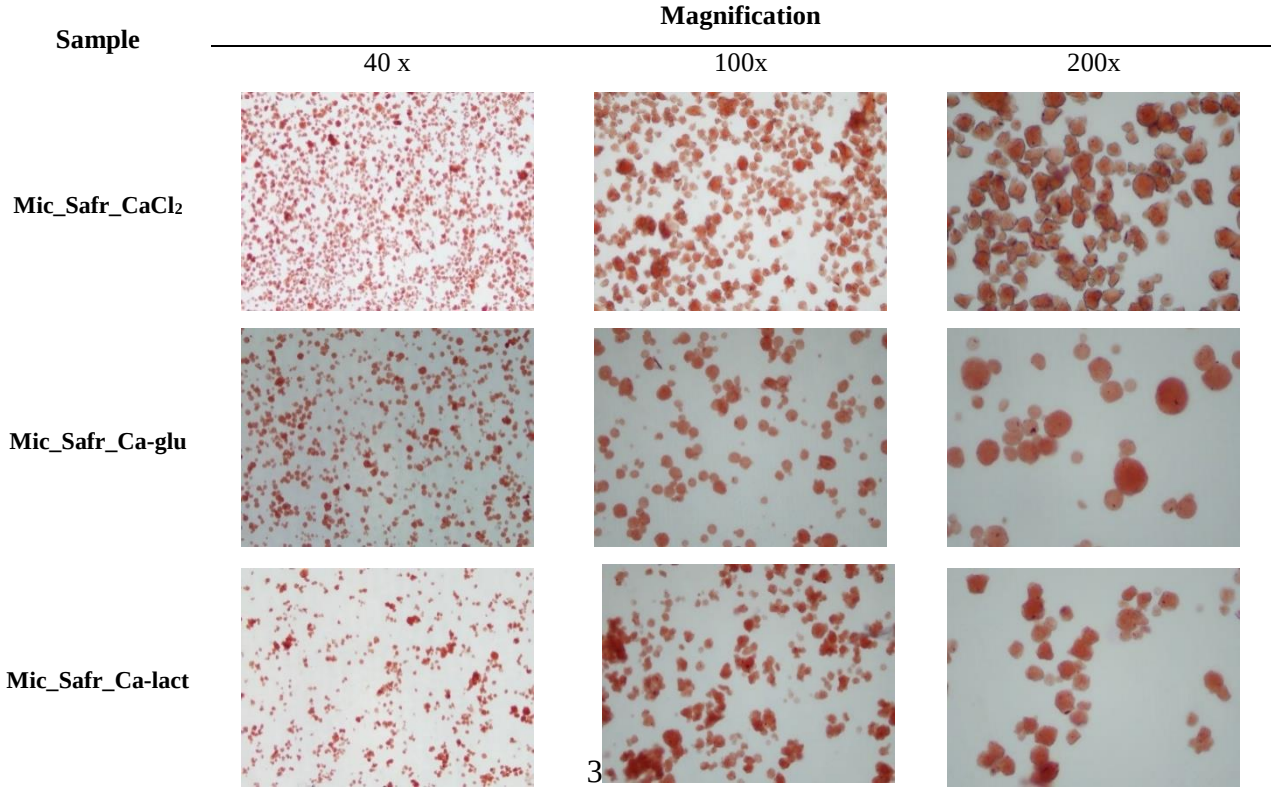

Figure 23 Safranin's MIC morphology after the rehydration capacity test.

4.1.5 FTIR analysis

The FTIR analysis was used to access the effective encapsulation of curcumin and safranin on the alginate matrix. Moreover, this analysis is also helpful to verify the chemical structure of the crosslinker on the freeze-dried MIC. The spectra are organized according to the used crosslinker, in the following sequence (up to bottom): alginate, crosslinker, empty MIC, active principle and MIC containing the active principles.

4.1.5.1 Alginate/$CaCl_2$/Active principle System

Figure 24 and 25 presents the FTIR spectra for Alginate, $CaCl_2$, MIC crosslinked with $CaCl_2$, pure curcumin and safranin, respectively, and MIC containing curcumin and safranin, respectively.

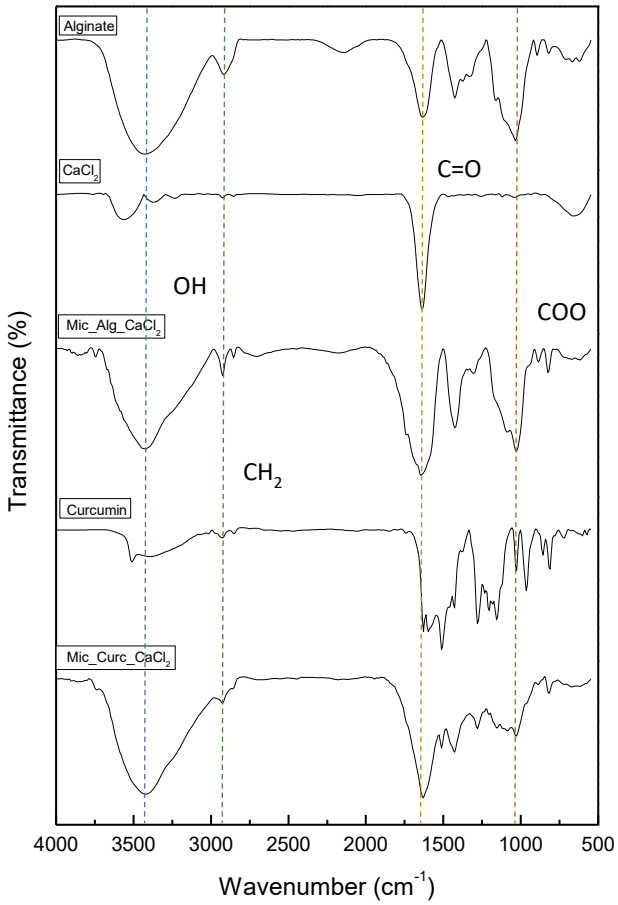

Figure 24 FTIR spectra of alginate, $CaCl_2$, empty MIC crosslinked with $CaCl_2$ pure curcumin and curcumin MIC crosslinked with $CaCl_2$.

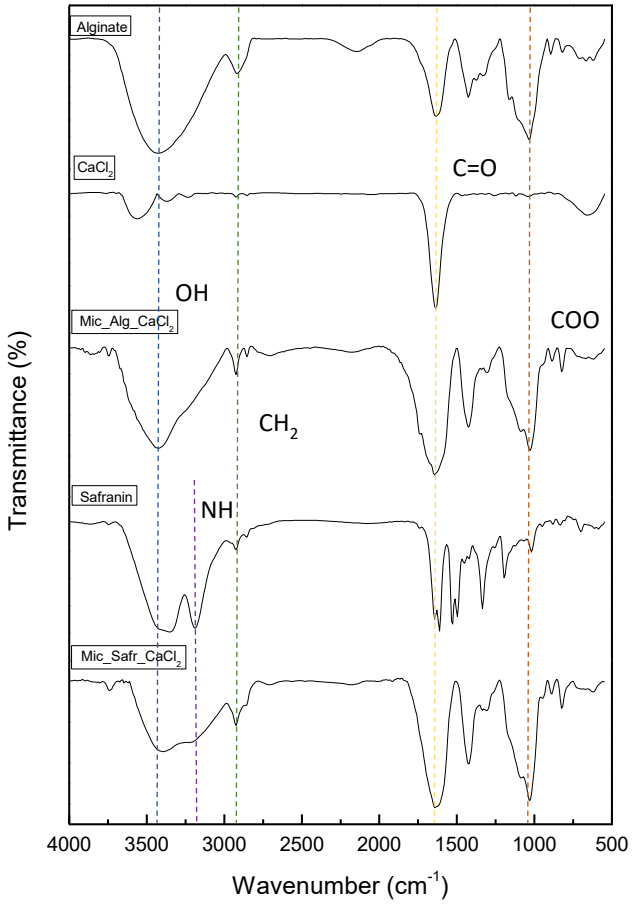

Figure 25 FTIR spectra of alginate, $CaCl_2$, empty MIC crosslinked with $CaCl_2$ pure safranin and safranin MIC crosslinked with $CaCl_2$.

Analyzing the spectra presented on figure 24 and 25, it can be observed:

- Some typical contributions can be detected in the alginate spectrum, namely: the peak around 1643 cm^{-1} is attributed to the C=O stretching vibrations, while the peak around 3409 cm^{-1} is related with the stretching vibrations of the hydroxyl groups. Moreover, the band identified at 1103 cm^{-1} corresponds to the ester group of alginates;
- For $CaCl_2$ spectra the, sharp peak around 1635 cm^{-1} and 3541 cm^{-1} correspond to the OH stretching and bending. According to Stuart (2004), the water molecules incorporated into the structure of crystalline compounds produces characteristic sharp brands in a range between 3800-3200 cm^{-1} and 1700-1600 cm^{-1}, due to the OH stretching and bending, respectively. This is in good agreement with the $CaCl_2$ used in this work, that has two water molecules on its structure;

- The empty microspheres spectra (Mic_Alg_$CaCl_2$) is dominated by the presence of alginate, where its contribution can be detected by the band corresponding to the COO groups at 1103 cm^{-1}. The peak around 1635 cm^{-1} corresponds to the sum of the peaks from alginate and $CaCl_2$, causing a widening of the band;
- For the curcumin, a contribution of free OH groups present in the aromatic rings are identified at 3510 cm^{-1}. The peak around 1627 cm^{-1} is attributed to the C=C symmetric aromatic ring stretching, while the peak at 1512 cm^{-1} is related with the C=O, and the peak around 1280 cm^{-1} is due to the C-O stretching from the ether group of curcumin. The FTIR spectrum of curcumin used in this study is similar to the spectra reported in the literature (Athira and Jyothi, 2014; Pawar, 2014);
- Regarding the safranin spectra, the peak at 3340 cm^{-1} is attributed to the OH groups, while the peak at 3186 cm^{-1} is assigned to the NH groups. The peak around 2923 cm^{-1} corresponds to de N-CH_2 stretching (Stuart, 2004);
- For the curcumin MIC, its contribution is identified at 1280 cm^{-1} and 1512 cm^{-1}, which the proves the effective encapsulation of curcumin. It is possible to observe the contribution of alginate in the vibration around 1627 cm^{-1} (C=O).
- For the safranin MIC, it can be observed that spectrum is dominated by the presence of alginate where is possible to identify the contribution of the carbonyl groups at 1643 cm^{-1}. Moreover, the contribution of the NH groups from safranin at 3271 $cm^{-1}$is also visible proving the safranin encapsulation.

4.5.1.2 Alginate/Ca-glu/Active principle System

Figure 26 and 27 presents the FTIR spectra for Alginate, Ca-glu, MIC crosslinked with Ca-glu, pure curcumin and safranin, respectively, and MIC containing curcumin and safranin, respectively.

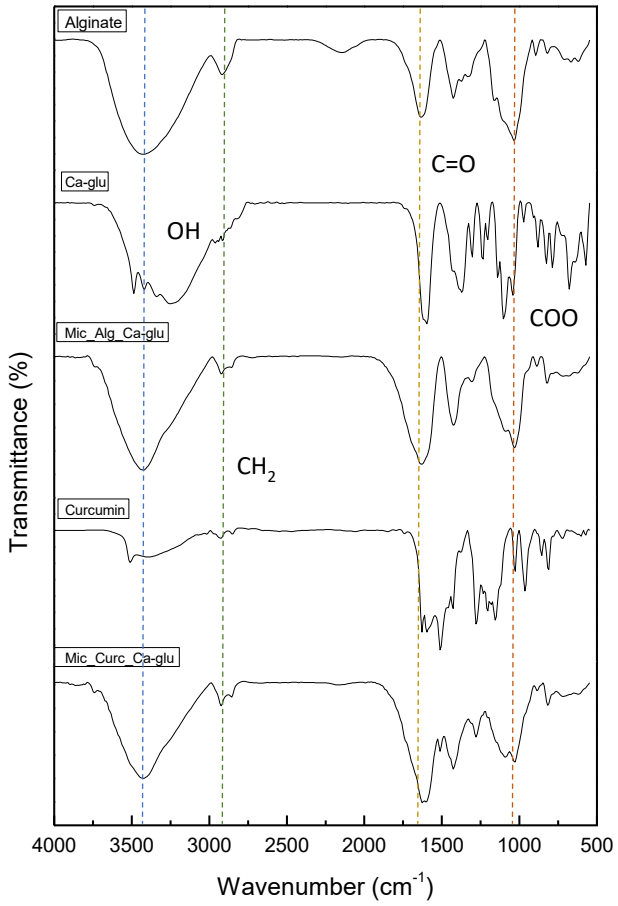

Figure 26 FTIR spectra of alginate, Ca-glu, empty MIC crosslinked with Ca-glu, pure curcumin and curcumin MIC crosslinked with Ca-glu.

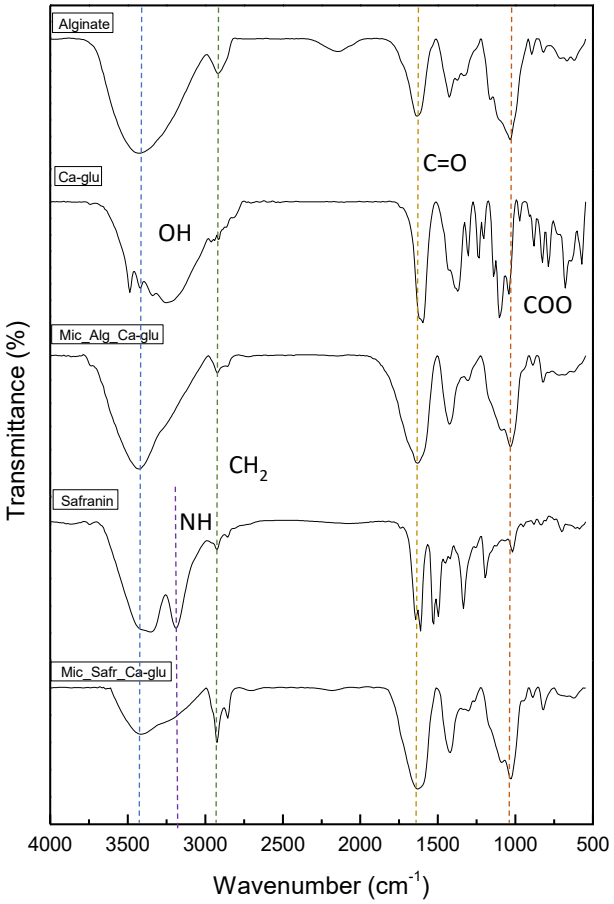

Figure 27 FTIR spectra of alginate, Ca-glu, empty MIC crosslinked with Ca-glu, pure safranin and safranin MIC crosslinked with Ca-glu.

Analyzing figure 26 and 27, it can be noticed:

- For the Ca-glu, the peak around 3263 cm^{-1} is related with the free OH groups while the peak at 1596 cm^{-1} is attributed to the carbonyl group. The peak around 1103 cm^{-1} corresponds to the ester group present in the compound;
- The empty MIC spectra is dominated by the presence of alginate, since two major features can be identified: the COO groups at 1103 cm^{-1} and the peak around 1590 cm^{-1}, corresponding to the carbonyl group;
- For the curcumin MIC, a major contribution of the alginate presence can be assigned, and it's possible to note the contribution of the carbonyl groups. The presence of Ca-glu is noticed at 1087 cm^{-1}(COO group), where a slight deformation of the peak is visible. Curcumin contribution is observed at 1512 cm^{-1} and 1280 cm^{-1}, which ensures that curcumin was encapsulated.

- For the safranin MIC sample, it is possible to observe the contribution of Ca-glu at 1087 cm^{-1}, which resulted on a small deformation in the characteristic band of COO derived from alginate spectra. The safranin contribution is observed at 3247 cm^{-1} (NH groups). However, it is possible to see that the MIC spectra is dominated by the presence of alginate.

4.5.1.3 Alginate/Ca-lact/Active principle System

Figure 28 and 29 presents the FTIR spectra for Alginate, Ca-lact, MIC crosslinked with Ca-lact, pure curcumin and safranin, respectively, and MIC containing curcumin and safranin, respectively.

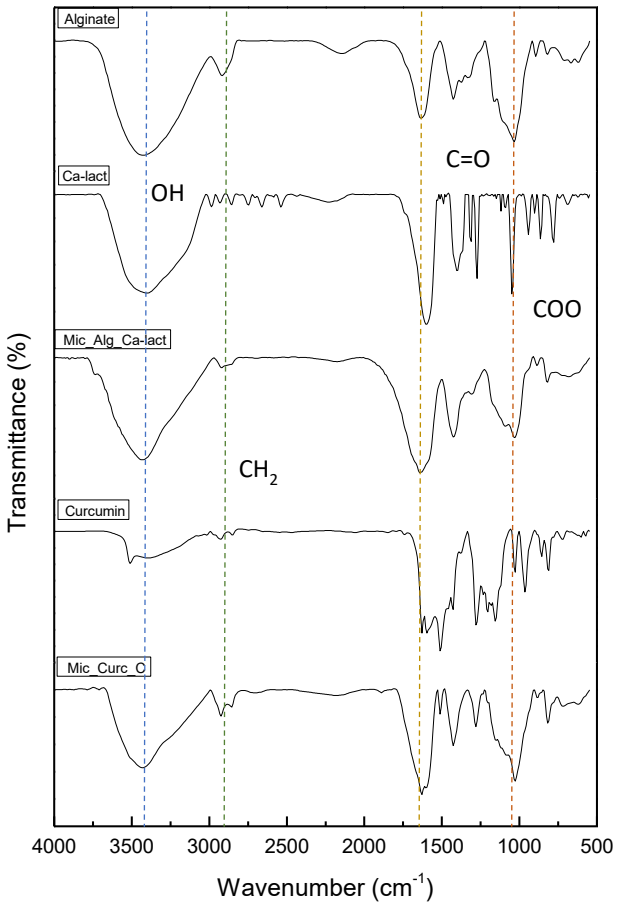

Figure 28 FTIR spectra of alginate, Ca-lact, empty MIC crosslinked with Ca-lact, pure curcumin and curcumin MIC crosslinked with Ca-lact.

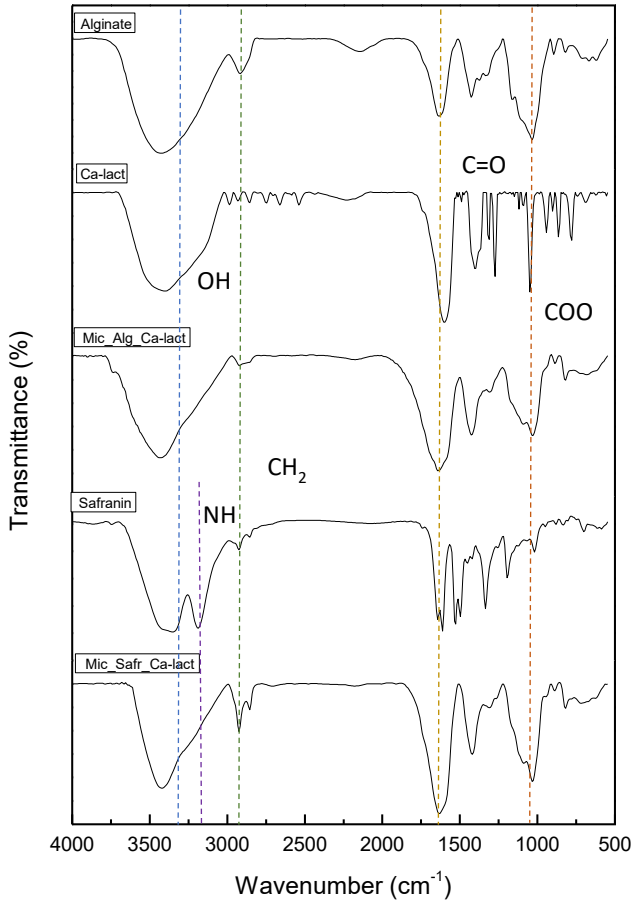

Figure 29 FTIR spectra of alginate, Ca-lact, empty MIC crosslinked with Ca-lact, pure safranin and safranin MIC crosslinked with Ca-lact.

From the observation of figure 28 and 29, it can be noticed:

- For the Ca-lact spectra, a peak around 3386 cm^{-1} is identified as the free OH groups contribution, and the peak around 1596 cm^{-1} its attributed to the C=O stretching vibrations. The sharp peak at 1396 cm^{-1} is related with the CH_3 bending vibrations, while the peak around 1049 cm^{-1} is due to the presence of the ester groups.
- The empty MIC spectra is also dominated by the presence of alginate, and it can be observed the contribution of alginate (COO groups at 1103 cm^{-1} and the peak around 1419 cm^{-1});
- For the curcumin MIC sample, the contribution of Ca-lact is observed at 1026 cm^{-1}, which causes a small deformation of the characteristic alginate peak (COO

groups). The peaks at 1512 and 1280 cm^{-1} are derived from curcumin, which proves that curcumin was encapsulated.

- For the safranin MIC spectra, the peak at 3163 cm^{-1} is assigned to the NH groups from safranin, which proves its encapsulation. The contribution of Ca-lact is observed at 1427 cm^{-1} and 1310 cm^{-1}, which corresponds to the CH_3 bending vibrations, which causes a small deformation of peak.

4.1.6 Release profile

This section is focused on the release profile of the active principles evaluation. Due to the curcumin hydrophobicity the release profile was studied using two different solvents: distilled water and ethanol, due to curcumin higher solubility in this former solvent. The release profile of safranin was studied only in distilled water. The active principle released was quantified by UV-vis analysis. Figure 30 shows the release profile of curcumin in distilled water.

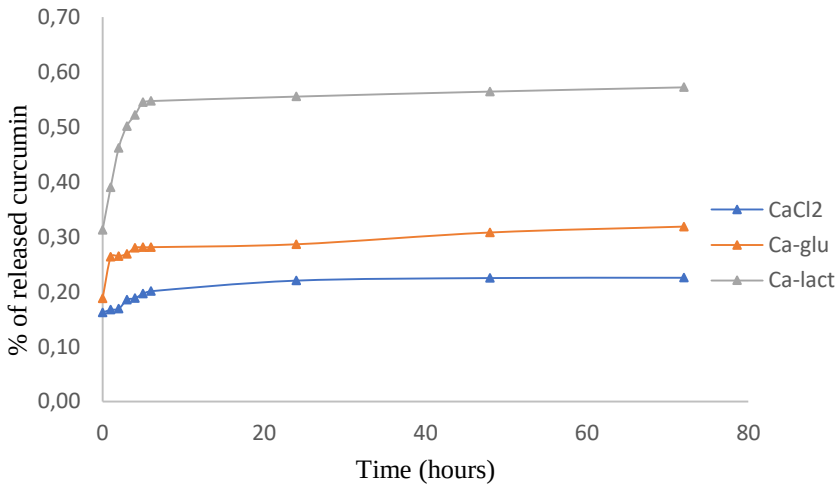

Figure 30 Release profile of curcumin from the MIC crosslinked with the different calcium sources in distilled water.

Analyzing the release profile in water (Figure 30), it can be observed that the release is very low in all cases. For the $CaCl_2$ crosslinked MIC the maximum release achieved was 0.22%, being followed by 0.31% for the Ca-glu crosslinked MIC and 0.57% for the Ca-lact crosslinked MIC. Considering that these release profiles were studied by using water as the solvent, these values are acceptable due to the curcumin hydrophobicity, not having

any affinity with water. For this reason, a second release study was done, using in this case ethanol as solvent due to the higher solubility presented for curcumin. The correspondent release profile is presented in Figure 31.

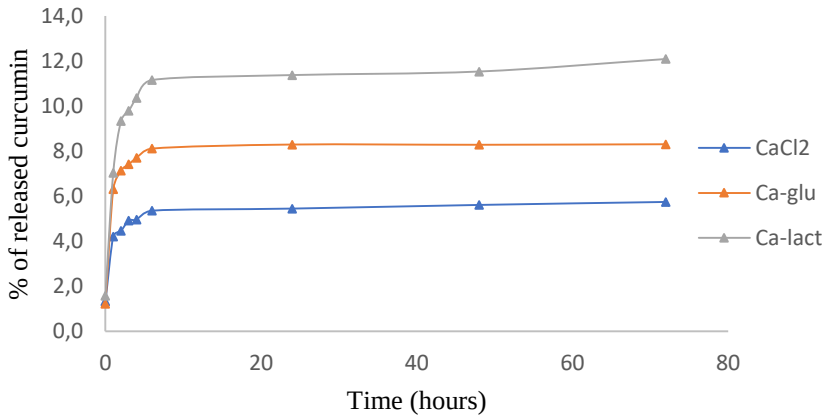

Figure 31 Release profile of curcumin from the MIC crosslinked with the different calcium sources in ethanol.

For the release profile in ethanol (Figure 31), a higher curcumin release was obtained when compared to the one registered for water, as expected. The maximum amounts of curcumin released for each used crosslinker were: 5.7%, for $CaCl_2$, 8.3% for Ca-glu and 12.1% for Ca-lact. Considering the high solubility of curcumin in ethanol, the amounts released can be consider as modest, once the maximum achieved release correspond to 12.1%. This difference can be due to the formation of curcumin crystals which have a lower solubility in ethanol. These crystal-like structures can be noticed in the OM images provided in Figure 16.

The safranin release in distilled water is shown in Figure 32. The maximum amounts of safranin released for each crosslinker used were: for $CaCl_2$ 4.15%, followed by 4.42% for Ca-glu and 4.76% for Ca-lact crosslinked MIC. These values were not expected, because safranin is a hydrophilic compound, and therefore, a large amount should be released for the water. One possible cause for this effect is related with the interaction between the alginate and safranin, since safranin has chlorine ion, and it can interact with the sodium ion from alginate in the presence water. This interaction might favor the entrapment of safranin inside the MIC, preventing its dissolution in water and thus the release. Regarding the curcumin release profile, it can be observed that the release reaches a plateau after approximately 6 hours, indicating that the release has reached to the

maximum. In the other hand, the release profile of safranin showed that, after 72 hours of release, the profile is still growing, which means that safranin is released gradually, indicating that longer times implies a higher release of the substance. It is also possible to observe that in all release profiles, there is an almost exponential loss in the first hour of test. This is due to the active principle present on the MIC surface: when it comes in contact with the release solution, migrates, increasing the concentration of active principle in the medium.

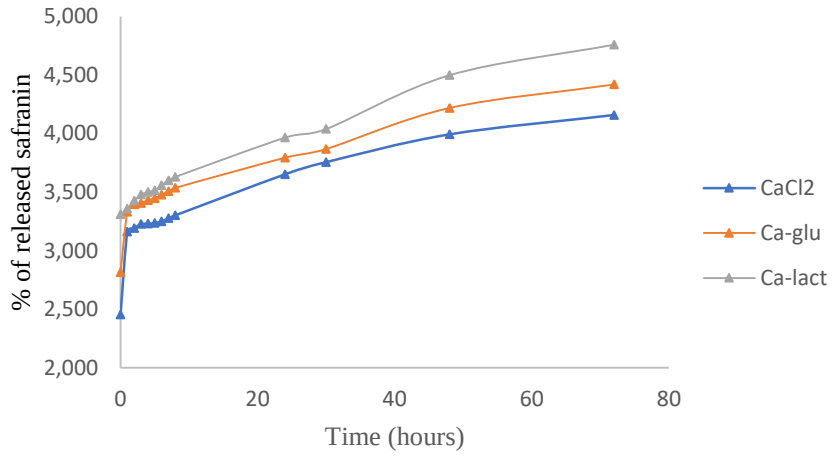

Figure 32 Release profile of safranin from the MIC crosslinked with the different calcium sources in distilled water

4.1.7 Particle size

Regarding the MIC particle size measurement, Figure 33, 34 and 35 show the particle sizes distributions in volume and in number of the particles produced by the spray-coagulation method after freeze-drying process. The mean values of the particle size distribution and the percentiles D_{10}, D_{50} and D_{90} are described in Tables 22, 23 and 24. The percentiles values represent the maximum particle size of 10%, 50% and 90% of the MIC, for each distribution (volume or number of particles). Additionally, in order to evaluate the particle size heterogeneity, the span was also calculated based on the D_{10}, D_{50} and D_{90} values of the volume distribution. The span is calculated by the equation (4).

$$\text{Span} = \frac{D_{90} - D_{10}}{D_{50}} \qquad \text{Eq. (4)}$$

2.1.1 $CaCl_2$ System

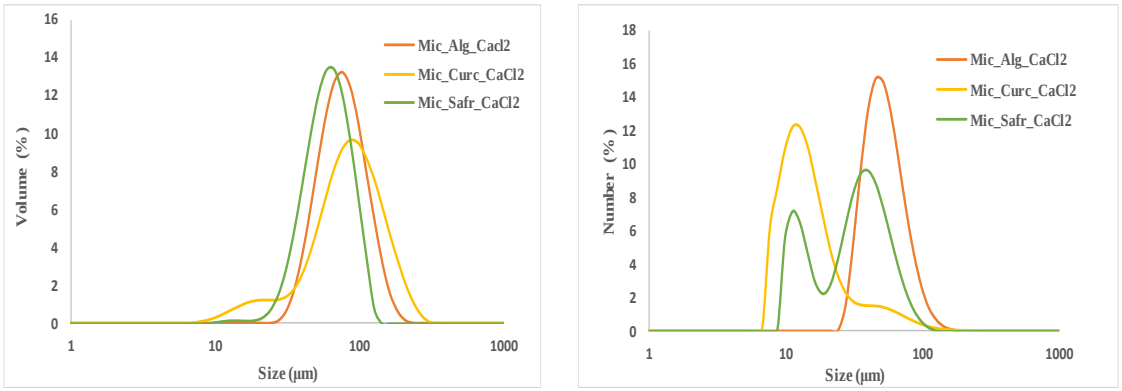

Figure 33 Particle size distributions of MIC crosslinked with CaCl2: (a) volume distribution and (b) number distribution.

Analyzing the particle size distributions in volume (Figure 33 (a)), a bimodal pattern is identified for the sample Mic_Curc_$CaCl_2$, while for the other two samples (Mic_Alg_$CaCl_2$ and Mic_Safr_$CaCl_2$) these distributions are unimodal. Regarding to the number distributions (Figure 33 (b)), for the empty MIC (Mic_Alg_$CaCl_2$) a unimodal pattern is noticed, while for the sample Mic_Curc_$CaCl_2$ proximately unimodal and for Mic_safr_$CaCl_2$ a bimodal distribution is noticed. The D_{10}, D_{50} and D_{90} values determined based on both number and volume distributions are described on Table 22. The D_{10} and D_{90} percentiles values of the Mic_Alg_$CaCl_2$ volume distribution were 49.5 and 130 µm,

and the mean particle size calculated based on this distribution was 80.31 μm. In the same manner, for the volume distribution of the sample Mic_Curc_$CaCl_2$ the D_{10} and D_{90} were 35.8 to 169 μm (mean size of 91.65 μm), while for the Mic_Safr_$CaCl_2$ were 39.2 to 101 μm (mean size of 61.10 μm).

Table 22 Values of D_{10}, D_{50}, and D_{90} for the volume and number distribution of the MIC crosslinked with $CaCl_2$.

	Volume distribution			Number distribution		
Sample	D_{10} (μm)	D_{50} (μm)	D_{90} (μm)	D_{10} (μm)	D_{50} (μm)	D_{90} (μm)
Mic_Alg_$CaCl_2$	49.5±0.134	80.1±0.163	130±0.564	36.9±0.145	54.2±0.159	86.0±0.145
Mic_Curc_$CaCl_2$	35.8±0.038	89.7±0.186	169±0.919	9.16±0.007	14.4±0.023	36.7±0.122
Mic_Safr_$CaCl_2$	39.2±0.205	65±0.256	101±0.544	12.2±0.091	35.5±0.455	64.9±0.390

Values expressed as mean ± standard deviation

2.1.2 Ca-glu System

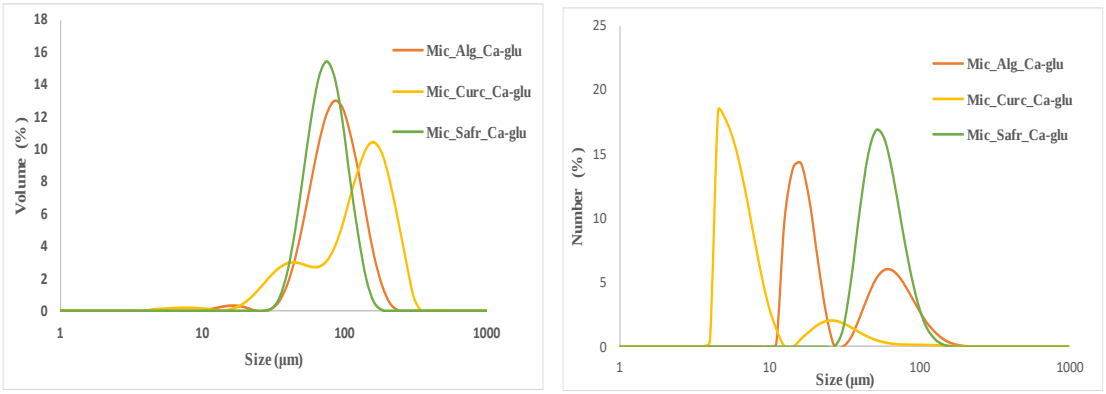

Figure 34 Particle size distribution of the MIC crosslinked with Ca-glu :(a) volume distribution and (b) number distribution.

Analyzing the particle size distributions in volume (Figure 34 (a)), a bimodal pattern is identified for the sample Mic_Curc_Ca-glu, while for the Mic_Alg_Ca-glu the distribution is proximately unimodal and for the Mic_Curc_Ca-glu is unimodal. Regarding to the number distributions (Figure 34(b)), for the MIC_Alg_Ca-glu and the Mic_Curc_Ca-glu a bimodal pattern is noticed, while for the sample Mic_Safr_Ca-glu a unimodal distribution is observed. The D_{10}, D_{50} and D_{90} values determined based on both number and volume distributions are described Table 23. The D_{10} and D_{90} percentiles values of the MIC_Alg_Ca-glu volume distribution were 55.4 to 149 μm (mean size of

91.46 µm). In the same manner, for the volume distribution of the sample Mic_Curc_Ca-glu the D_{10} and D_{90} were 40.5 to 239 µm (mean size of 131.46 µm), while for the Mic_Safr_Ca-glu were and 53 to 121 µm (mean size of 78.85 µm).

Table 23 Values of D_{10}, D_{50}, and D_{90} for the volume and number distributions for the MIC crosslinked with Ca-glu.

	Volume Distribution			Number distribution		
Sample	D_{10} (µm)	D_{50} (µm)	D_{90} (µm)	D_{10} (µm)	D_{50} (µm)	D_{90} (µm)
Mic_Alg_Ca-glu	55.4±0.286	92.1±0.371	149±0.789	12.7±0.045	18.8±0.212	79.7±0.721
Mic_Curc_Ca-glu	40.5±0.118	140±0.957	239±0.713	4.90±0.006	6.61±0.029	26.0±0.081
Mic_Safr_Ca-glu	53.0±0.160	80.3±0.283	121±0.473	41.8±0.131	59.5±0.210	90.1±0.341

Values expressed as mean ± standard deviation.

2.1.3 Ca-lact System

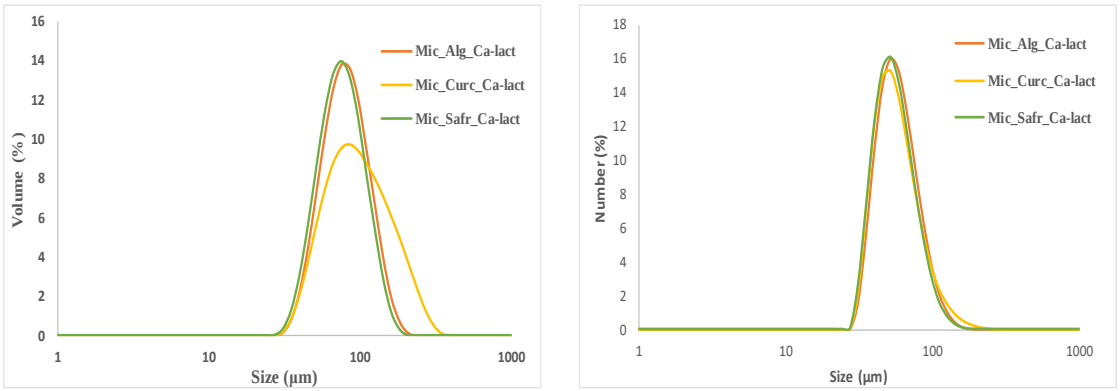

Figure 35 Particle size distribution of the MIC crosslinked with Ca-lact: (a) volume distribution and (b) number distribution.

From the analysis of the particle size distributions in volume (Figure 35 (a)), a unimodal pattern is identified all the three samples, while the same is observed for the number distribution in all the cases. The D_{10}, D_{50} and D_{90} values determined based on both number and volume distributions are described Table 24. The D_{10} and D_{90} percentiles values of the Mic_Alg_Ca-lact volume distribution were 54 to 135 µm (mean size of 84.78 µm). In the same manner, for the volume distribution of the sample Mic_Curc_Ca-lact the D_{10} and D_{90} were 56.1 to 202 µm (mean size of 108.9 µm), while for the Mic_Safr_Ca-glu were and 51.6 to 126 µm (mean size of 79.87 µm).

Table 24 Values of D_{10}, D_{50}, and D_{90} for the volume and number distribution of the MIC crosslinked with Ca-lact

	Volume Distribution			Number distribution		
Sample	D_{10} (μm)	D_{50} (μm)	D_{90} (μm)	D_{10} (μm)	D_{50} (μm)	D_{90} (μm)
Mic_Alg_Ca-lact	54.0±0.376	85.1±0.199	135±0.564	41.5±0.405	59.7±0.602	93.5±0.473
Mic_Curc_Ca-lact	56.1±0.277	102±0.687	202±1.10	40.6±0.144	58.3±0.238	97.8±0.462
Mic_Safr_Ca-lact	51.6±0.221	80.8±0.275	126±0.425	40±0.237	57.0±0.214	88.8±0.365

Values expressed as mean ± standard deviation.

Having in view the evaluation of the samples particle size homogeneity, the span value was calculated for all the MIC samples, based on the volume size distributions. The obtained values are described on Table 25. Based on the span, it can be concluded that all the curcumin samples (Mic_Curc_$CaCl_2$, Mic_Curc_Ca-glu and Mic_Curc_Ca-lact) have higher size and heterogeneous character in comparison with the other samples, once the values were all above 1.4. This feature is related with the curcumin suspension used for the MIC production. This means that these MIC inners are composed by curcumin suspended particles on the aqueous alginate solution, generating particles with larger sizes. In the case of safranin MIC (Mic_Safr_$CaCl_2$, Mic_Safr_Ca-glu and Mic_Safr_Ca-lact) a homogenous character is evidenced by the span values lower than 1.0. This can be associated with the safranin's hydrophilic nature that allows a homogeneous dispersion on the alginate matrix, having no influence on the particle size.

Considering the differences of the particle size distributions between the three used calcium sources, it can be observed that all the MIC samples follow the same pattern: curcumin MIC have the larger mean particle size and safranin the smallest one. Regarding to the spray-coagulation method most significant variable is the size of the drops generated during the spraying stage are the solution/suspension flow rate, the gas pressure, the nozzle diameter (0.35 mm, in this case) and the height relatively to the coagulation solution surface. Furthermore, from the particles size results an unexpected effect related with the type of crosslinker was noticed. Analyzing the possible influence of the crosslinker chemical structures, it was firstly expected that no influence was observed, once only the dissociated calcium interacts with the alginate MIC. However, the results point for a possible influence of the ions chemical structure (lateral molecular

chains) that were generated from the calcium sources dissociation (after the Ca^{2+} release). This assumption requires further studies in order to be properly evaluated.

Regarding to the Ca-glu crosslinked MIC, larger mean particle sizes are registered than for the remaining samples. This can be due to the MIC agglomeration effect detected on the OM analysis at the end of the production of the MIC crosslinked with calcium gluconate. Oppositely, the MIC crosslinked with Ca-lact presented the lower span values, once the particle sizes distributions were unimodal in all cases.

Table 25 Span values determined based on the volume distributions.

Sample	Span	Sample	Span	Sample	Span
Mic_Alg_$CaCl_2$	1.0049	Mic_Alg_Ca-glu	1.0162	Mic_Alg_Ca-lact	0.9518
Mic_Curc_$CaCl_2$	1.4849	Mic_Curc_Ca-glu	1.4178	Mic_Curc_Ca-lact	1.4303
Mic_Safr_$CaCl_2$	0.9507	Mic_Safr_Ca-glu	0.8468	Mic_Safr_Ca-lact	0.9207

4.1.8 Thermogravimetric analysis

4.1.8.1 Analysis of the individual compounds

The TGA analysis was used to check the thermal stability of the freeze-dried microspheres (empty, with curcumin and safranin) crosslinked with the three calcium sources ($CaCl_2$, Ca-glu and Ca-lact). Pure alginate, curcumin and safranin were also analyzed, being the individual thermograms presented in Figure 36. Table 26 shows a summary of the sample analysis (mass loss and maximum degradation temperature).

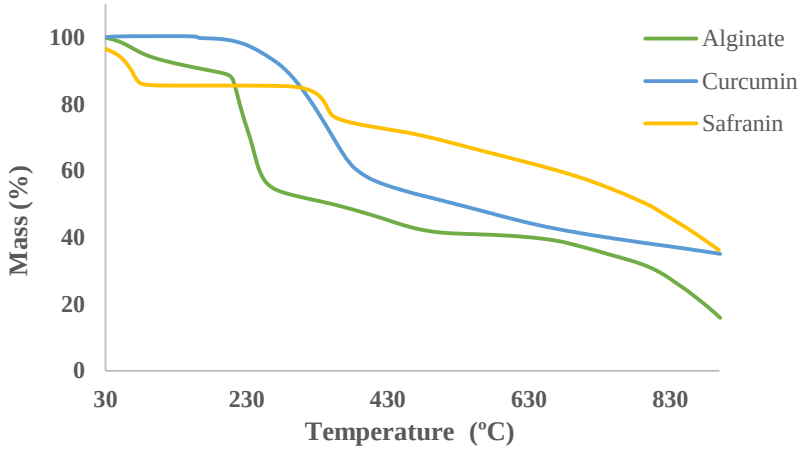

Figure 36 Results of the thermogravimetric analysis of pure alginate, curcumin and safranin.

From sodium alginate thermogram, four degradation regions can be identified: 32-110ºC, 187-229ºC, 300-520ºC, and the last one, above 600ºC. The first region corresponds to the water loss (around 10.21%). The second region, where a 37.90% of weight loss is registered, corresponding to the rupture of alginate fragments and monomer chains (Kragovic et al., 2016) . The third region (300-520ºC), corresponds to the break of the alginate glycoside bonds, causing a weight loss of 10.93%. According Pathak et al. (2010), the final step of the degradation (600-800ºC) might be attributed to the formation of carbonate salts, being resultant from the association of the Na with CO_3 molecules, causing a weight loss of 9.48%. The final residue obtained at 900 ºC was 16.26%.

Regarding the curcumin thermogram, no water loss is observed due to its hydrophobic nature. Curcumin starts to decompose at 255ºC and the maximum degradation temperature was 347ºC, which corresponds to a mass loss of 46.97%. Finally, a residue of 35.06% is registered.

Analyzing the safranin thermogram, it is possible to observe two different regions: the first one in the region 32-116ºC, which corresponds to the water loss (weight loss of 11.04%) and a second region, starting at 276ºC with a maximum degradation temperature of 414ºC, corresponding to a mass loss of 12.28%. The final residue is 36.24%

Table 26 Summary of the alginate, curcumin and safranin TGA results

Sample	Sample mass (mg)	Water content ((w/w), %)	Initial Degradation Temperature (ºC)	Final Residue ((w/w),%)
Alginate	6.59	10.21	189	16.26
Curcumin	6.04	0.00	255	35.06
Safranin	6.64	11.04	276	36.24

4.1.8.2 Analysis of the empty Microspheres

Figure 37 shows the thermograms of the empty alginate microspheres crosslinked with the three different calcium sources ($CaCl_2$, Ca-glu and Ca-lact).

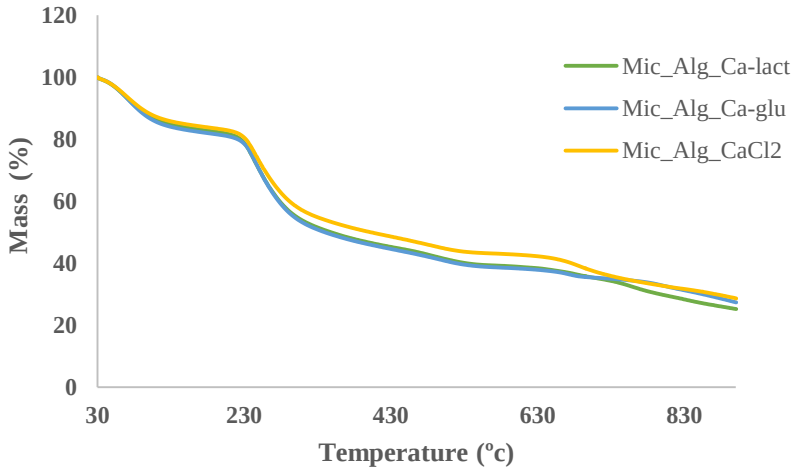

Figure 37 Thermogravimetric analysis of the empty microspheres crosslinked with the three different calcium sources.

Analyzing the obtained thermograms, it is possible to observe that for the three samples a similar pattern is observed. The first region (32-180ºC) corresponds to the free water elimination, with a weight loss of 15.86% for Mic_Alg_$CaCl_2$, 17.54% for Mic_Alg_Ca-glu and 16.76% for Mic_Alg_Ca-lact. Different authors reported that hydrophilic polymers have three different kinds of absorbed water: free, freezing bound and non-freezing bound water (Pathak et al., 2010; Russo et al., 2007). Free water does not interact with the polymer molecules and is the first one to be removed from the polymer (until 100 ºC). The freezing bound water has a weakly interaction with the polymer chains and

is removed in the second place, whereas the non-freezing bound forms hydrogen bonds with the polymer chain and is the latest to decompose, requiring higher temperatures until 180ºC). The second region, comprised between 180-255ºC corresponds to the alginate degradation. For the Mic_Alg_Ca-glu this region starts at 247ºC, while for Mic_Alg_Ca-lact a temperature of 248ºC is registered, whereas for the Mic_Alg_$CaCl_2$, 252ºC was observed. These results show that the increment of the alginate degradation temperature (229ºC) due to the crosslinking with Ca^{2+} is compatible with an increasing thermal stability. The weight loss associated to the alginate degradation was 32.5% for Mic_Alg_$CaCl_2$, 36.24% for Mic_Alg_Ca-glu and 36.13% for Mic_Alg_Ca-lact. The degradation stage after 400ºC is also related with the break of the glyosidic chain (Patel et al., 2016), corresponding to a weight loss of 5.42% for Mic_Alg_Ca-lact, 5.62% for Mic_Alg_Ca-glu and 5.89% for Mic_Alg_$CaCl_2$. The weight loss observed between 600-800ºC is due to the formation carbonate salts, whereas Mic_Alg_Ca-lact has a weight loss of 3.12%, followed by Mic_Alg_$CaCl_2$ with 3.72% and 4.14% for Mic_Alg_Ca-glu (Table 27). In order to estimate the Ca^{2+} content present in each empty MIC sample, a calculation based on the difference of the final residue obtained for these samples and the one registered for pure alginate was made. The results are described on Table 27. Based on these results, a Ca^{2+}residue of 12.52% was obtained for the Mic_Alg_$CaCl_2$, while for the Mic_Alg_Ca-lact this value was 11.11% and for the Mic_Alg_Ca-glu a 9.08% of Ca^{2+} was registered. These results pointed out for a higher content of Ca^{2+} on the $CaCl_2$ crosslinked Mic, being followed by the Ca-lact and finally the Ca-glu ones, being the Mic_Ca-lact close to the Mic_Ca-glu, comparatively to the $CaCl_2$.

Table 27 Estimation of the Ca^{2+} content present in three empty MIC samples.

Sample	Sample mass (mg)	Water content ((w/w),%)	Initial Degradation temperature (ºC)	Final Residue ((w/w), %) (900ºC)	Ca^{2+} residue ((w/w), %)
Mic_Alg_$CaCl_2$	6.29	15.86	252	28.78	12.52
Mic_Alg_Ca-glu	6.47	16.87	247	25.28	9.08
Mic_Alg_Ca-lact	6.40	18.16	248	27.37	11.11

4.1.8.3 Analysis of the $CaCl_2$ System

Figure 38 shows the thermograms of the alginate microspheres containing curcumin and safranin crosslinked with $CaCl_2$. Herein a first region (32-190ºC) corresponds to a weight loss of 14.85% due to the water removal, for the Mic_Curc_$CaCl_2$, and 16.18% for Mic_Safr_$CaCl_2$. The second region (200-400ºC) corresponds to the alginate degradation, leading to a weight loss of 29.14% for Mic_Curc_$CaCl_2$ and 34.80% for Mic_Safr_$CaCl_2$. For Mic_Curc_$CaCl_2$, curcumin degradation causes a weight loss of 6.79% in a range of temperatures between 350-444ºC. The increase of curcumin's degradation temperature is justified by the fact that it is protected by the alginate matrix, which causes an increased thermal stability. The same phenomena is verified for the safranin degradation once a weight loss of 6.34% is detected in the temperatures range between 400 and 550ºC approximately. Table 28 shows the thermal parameters for the microspheres crosslinked $CaCl_2$ containing curcumin and safranin.

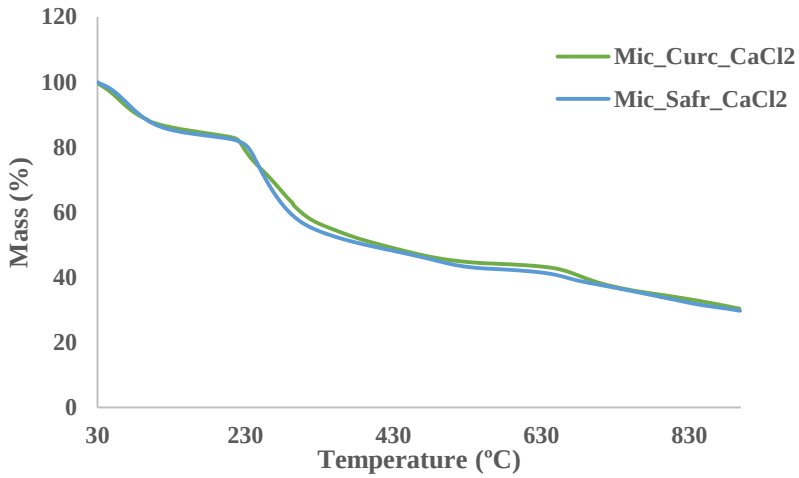

Figure 38 Thermogravimetric analysis of the alginate microspheres containing curcumin and safranin, crosslinked with $CaCl_2$.

Table 28 Thermal properties of the curcumin and safranin microspheres crosslinked $CaCl_2$

Sample	Sample mass (mg)	Water content ((w/w), %)	Initial Degradation Temperature (ºC)	Final Residue ((w/w), %) (900ºC)
Mic_Curc_$CaCl_2$	6.25	15.45	187	30.36
Mic_Safr_$CaCl_2$	6.46	16.83	192	29.71

4.1.8.4 Analysis of Ca-glu System

Figure 39 shows the thermograms of alginate microspheres containing curcumin and safranin, crosslinked with Ca-glu, where a similar thermal behavior of both samples is identified. The first region is due to the water removal, causing a weight loss of 16.31% for Mic_Safr_Ca-glu and 12.78% for Mic_Curc_Ca-glu. The second one corresponds to alginate degradation, with 34.38% of weight loss for Mic_Safr_Ca-glu and 30.20% for Mic_Curc_Ca-glu. Curcumin degradation occurs between 330ºC and 415ºC, causing a weight variation of 8.05%. For safranin, the degradation process starts at around 355ºC until 497ºC, causing a weight loss of 7.18%. Once again, the increasing of the active principles thermal stability is associated with the protective action of the alginate matrix. Table 29 presents the thermal parameters for the microspheres crosslinked Ca-glu containing curcumin and safranin.

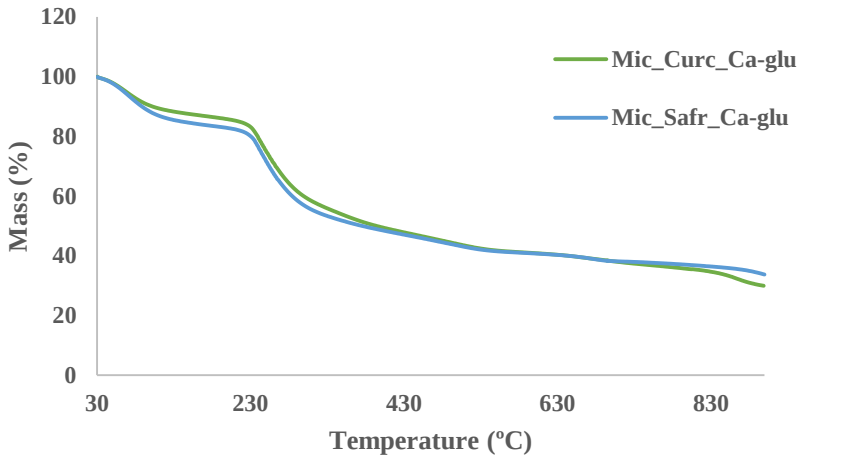

Figure 39 Thermogravimetric analysis of the alginate microspheres containing curcumin and safranin, crosslinked with Ca-glu.

Table 29 Thermal properties of the curcumin and safranin microspheres crosslinked with Ca-glu.

Sample	Sample mass (mg)	Water content ((w/w), %)	Initial Degradation Temperature (ºC)	Final Residue ((w/w),%) (900ºC)
Mic_Curc_Ca-glu	6.32	13.13	192	29.97
Mic_Safr_Ca-glu	6.46	16.83	175	33.74

4.1.8.5 Analysis Ca-lact System

Figure 40 shows the thermograms of alginate microspheres containing curcumin and safranin, crosslinked with Ca-lact, where a similar degradation profile for both samples can observed. The first degradation region (from 32ºC to 194ºC) corresponds to the water removal. The second region is identified as the alginate degradation (between 194ºC and 400º), causing a weight loss of 31.14% for Mic_Curc_Ca-lact and 36.31% for Mic_Safr_Ca-lact. Curcumin degradation occurs between 320ºC and 400ºC, where a weight loss of 7.89% is obtained while safranin degradation takes place between 420ºC and 571ºC, causing a weight loss of 6.66%

Table 30 presents the thermal parameters for the microspheres crosslinked Ca-lact containing curcumin and safranin.

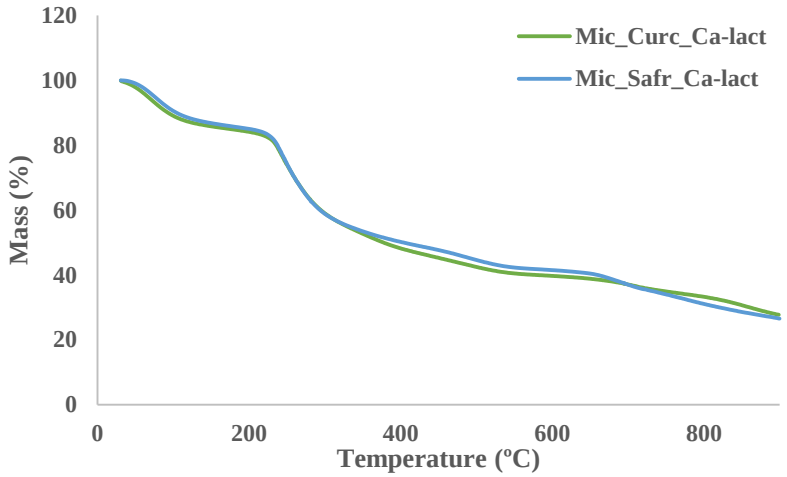

Figure 40 Thermogravimetric analysis of the alginate microspheres containing curcumin and safranin, crosslinked with Ca-lact.

Table 30 Thermal properties of the curcumin and safranin microspheres crosslinked with Ca-lact

Sample	Sample mass (mg)	Water content ((w/w),%)	Initial Degradation Temperature (ºC)	Final Residue ((w/w),%) (900ºC)
Mic_Curc_Ca-Lat	6.60	14.50	159	27.72
Mic_Safr_Ca-Lact	6.52	14.56	188	26.52

4.2 Microencapsulation of a hydrophobic and hydrophilic active principle using superhydrophobic surfaces

This section is related to the studies of curcumin and safranin microencapsulation by using the superhydrophobic surface (SH) methodology. Samples of 10 MIC crosslinked with the three calcium salts were made for each active principle. The samples were named according to the active principle, the used crosslinker, and the encapsulation method by using SH also included in the name. Thus "SH_Alg _$CaCl_2$, Ca-glu or Ca-lact" means "Empty alginate microspheres cross-linked with $CaCl_2$, Ca-Glu and Ca-Lact", respectively, "SH_Curc_$CaCl_2$, Ca-glu or Ca-lact" means "Curcumin microspheres crosslinked with $CaCl_2$, Ca-Glu and Ca-Lact", respectively and "SH_Safr_ $CaCl_2$, Ca-glu or Ca-lact" means "Safranin microspheres crosslinked with $CaCl_2$, Ca-Glu and Ca-Lact.

4.2.1 Optical Microscopy

Figure 41, 42, 43 and 44 shows the OM images of the curcumin and safranin's MIC crosslinked with the three calcium salts at t=0 (before the addition of the crosslinking solution), t=1, t=30 and t=60 min (after the addition of the crosslinking solution). The images were acquired on the SH surface, with a magnification of 40x.

Sample	t= 0 minutes	**Sample**	t= 0 minutes
SH_Curc_$CaCl_2$		**SH_Safr_ $CaCl_2$**	
SH_Curc_Ca-glu	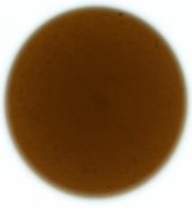	**SH_Safr_Ca-glu**	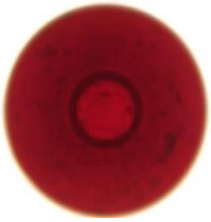
SH_Curc_Ca-lact		**SH_Safr_Ca-lact**	

Figure 41 Curcumin and safranin MIC produced on the SH surface (t=0 minutes).

Sample	t= 1 minute	Sample	t= 1 minute
SH_Curc_$CaCl_2$		**SH_Safr_$CaCl_2$**	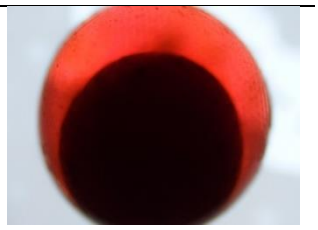
SH_Curc_Ca-glu	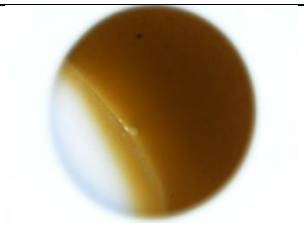	**SH_Safr_Ca-glu**	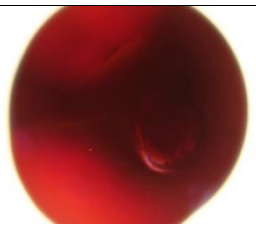
SH_Curc_Ca-lact		**SH_Safr_Ca-lact**	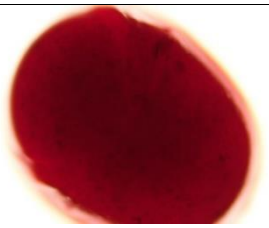

Figure 42 Curcumin and safranin MIC produced on the SH surface (t=1 minute).

Sample	t= 30 minutes	Sample	t= 30 minutes
SH_Curc_$CaCl_2$		**SH_Safr_ $CaCl_2$**	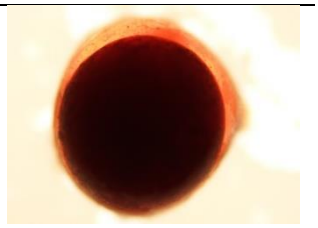
SH_Curc_Ca-glu		**SH_Safr_Ca-glu**	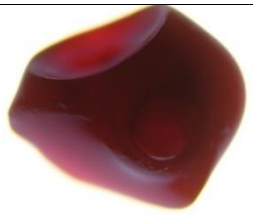
SH_Curc_Ca-lact	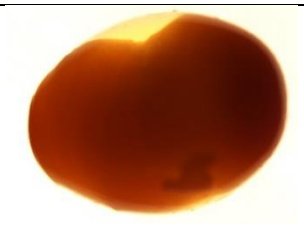	**SH_Safr_Ca-lact**	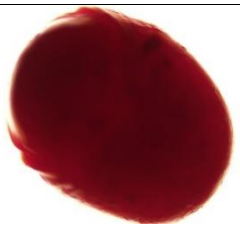

Figure 43 *Curcumin and safranin MIC produced on the SH surface (t=30 minutes).*

Sample	t= 60 minutes	Sample	t= 60 minutes
SH_Curc_$CaCl_2$		**SH_Safr_$CaCl_2$**	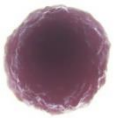
SH_Curc_Ca-glu		**SH_Safr_Ca-glu**	
SH_Curc_Ca-lact		**SH_Safr_Ca-lact**	

Figure 44 Curcumin and safranin MIC produced on the SH surface (t=60 minutes

By observing the images shown on Figure 41, the spherical conformation of the emulsion/solution drops after being placed on the SH surface can be clearly noticed. This perfect conformation is related with the repellency effect exerted by the SH surface. When the crosslinker solution is added, the drop starts to lose the spherical conformation, due to surface tensions. This effect is more pronounced for the curcumin MIC crosslinked with $CaCl_2$ and Ca-lact (SH_Curc_$CaCl_2$ and SH_Curc_Ca-lact, Figure 42). After 30 minutes (Figure 43), it still possible to observe the crosslinking solution on the MIC surface and a reduction in the MIC size caused by the water evaporation. Figure 44 shows the MIC aspect at the end of 1 hour of crosslinking, where small wrinkles are noticed on the particle surface. Regarding the curcumin MIC, a higher deformation degree is evidenced, comparatively with the safranin ones. Making a qualitative estimative for the EE, values of 100% can be considered, since there was no active principle loss for the surface during the entire process. This is one of the greatest advantages of this method, in particular when hydrophilic compounds are being encapsulated, comparatively with processes that use aqueous solutions as the coagulation baths. In order to guarantee the complete drying, the MIC were freeze-dried (Figure 45).

Sample		Sample	
SH_Curc_$CaCl_2$		**SH_Safr_ $CaCl_2$**	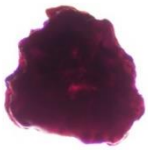
SH_Curc_Ca-glu	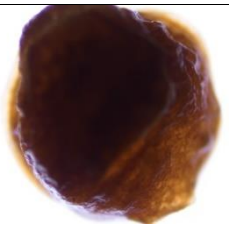	**SH_Safr_Ca-glu**	
SH_Curc_Ca-lact	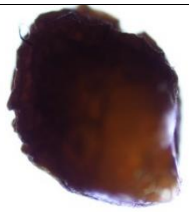	**SH_Safr_Ca-lact**	

Figure 45 Curcumin and safranin MIC produced on the SH surface, after freeze-drying.

4.2.2 Dry Residue

Table 31 and 32 describe the MIC mass after the production and after being freeze dried, and the corresponding calculated dry residue % (w/w).

Table 31 Microencapsulation of curcumin in alginate crosslinked with different calcium sources, produced in the SH surface.

Sample	Weight of wet MIC (n=10) (mg)	Weight of dry MIC (n=10) (mg)	Dry Residue % (w/w)
SH_Curc _ $CaCl_2$	57	5.1	8.97
SH_Curc_Ca-glu	47	4.6	9.78
SH_Curc_Ca-lact	41	4.2	10.24

Table 32 Microencapsulation of safranin in alginate crosslinked with different calcium sources, produced in the SH surface

Sample	Weight of wet MIC (n=10) (mg)	Weight of dry MIC (n=10) (mg)	Dry Residue % (w/w)
SH_Safr _$CaCl_2$	52	4.1	7.88
SH_Safr_Ca-glu	51	4.2	8.23
SH_Safr_Ca-lact	48	4.4	9.16

4.2.3 Rehydration capacity

The rehydration capacity was evaluated to check the MIC ability to recover the initial shape. For this assay, the freeze-dried MIC were put in 10 ml of water for 72 hours, being afterwards weighed. Tables 33 and 34 shows the weight of the samples before and after the test, as well the rehydration capacity value (% w/w). Analyzing the results, it can be observed that the MIC crosslinked with Ca-glu have a good rehydration capacity in both cases, followed by the MIC crosslinked with Ca-lact and the MIC crosslinked with $CaCl_2$. Comparing these results with the rehydration capacity of the MIC produced using the spray-coagulation method (Tables 20 and 21), it can be observe that they follow the same trend, with the MIC crosslinked with Ca-glu having better capacity to rehydrate.
Figure 46 shows curcumin and safranin MIC aspect, after the rehydration capacity test (72h).

Table 33 Rehydration capacity results for curcumin MIC produced on SH surface.

Sample	MIC Intial weight t=0 (mg)	MIC final weight t=72h (mg)	Rehydration capacity (% w/w)
SH_Curc_$CaCl_2$	57	24.1	42.28
SH_Curc_Ca-glu	47	39.2	83.40
SH_Curc_Ca-lact	41	22.1	53.90

Table 34 Rehydration capacity results for safranin microspheres produced on SH surfaces.

Sample	MIC Initial weight t=0 (mg)	MIC Final weight t=72h (mg)	Rehydration capacity (% w/w)
SH_Safr_$CaCl_2$	52	19.1	36.53
SH_Safr_Ca-glu	51	43.4	85.09
SH_Safr_Ca-lact	48	27.6	57.51

Sample	t= 72 hours	**Sample**	t= 72 hours
SH_Curc_$CaCl_2$		**SH_Safr_$CaCl_2$**	
SH_Curc_Ca-glu	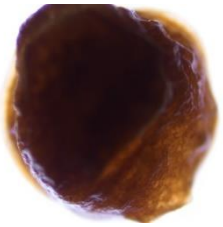	**SH_Safr_Ca-glu**	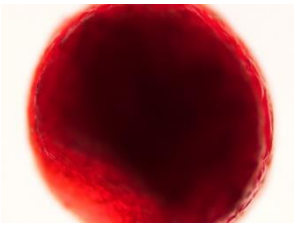
SH_Curc_Ca-lact	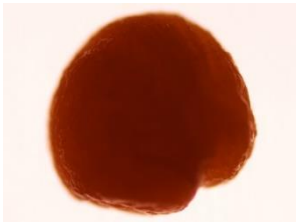	**SH_Safr_Ca-lact**	

Figure 46 Curcumin and safranin MIC produced on the SH surface, after the rehydration capacity test (72 hr).

4.3 Alginate crosslinking with different calcium sources: critical analysis of the results

Having in view the discussion of calcium sources effect, calcium chloride, calcium gluconate and calcium lactate, on the EE, rehydration capacity and on the release profile, this section is devoted to the analysis of the parameters which present a major role on the MIC crosslinking process when using the spray-coagulation method.

It is well known that the alginate crosslinking with Ca^{2+} is achieved by the ionic crosslinking of the calcium ions with the carboxyl groups of the guluronic acid (G residues). In the spray coagulation method, the variables that influence this reaction are:

(1) The calcium dissociation on the coagulation solution, being this dependent on the pK_a values of the substance. According to Clayden et al. (2001), the pK_a of an acid is the pH where it is exactly half dissociated. At pH above the pK_a, the substance is dissociated whereas at pH below the pK_a the substance is undissociated. Based in the values of pH and pK_a of each solution described on Table 35, and considering the conditions used on the present work, namely calcium source concentration on the coagulation solution (4% (w/v)) and alginate solution concentration (4% (w/v)), it can be stated that all the compounds are in conditions that favors their dissociation. It is worth to mention that when a total dissociation of the calcium salts occurs, the molecular side chain of Ca^{2+} are lost, rendering a free calcium ion. This means that the chemical structures of the calcium salts do not play a direct influence on the alginate crosslinking.

(2) The calcium diffusion to the inner particle and Ca^{2+} concentration on the coagulation solution. According to Lee and Rogers (2012), the rate of diffusion of Ca^{2+} depends directly on the concentration present in the solution. For the system alginate:$CaCl_2$ the molar ratio between the Ca^{2+}/G of alginate is equal to 45 (Table 35), this means that a $CaCl_2$ solution at 4% (w/v) has a Ca^{2+} concentration 45-fold higher than the required for the alginate crosslinking. This factor ensures a good rate of Ca^{2+} diffusion into the MIC, resulting in a more effective alginate crosslinking and leading to a good entrapment of the active principle inside the matrix. Regarding the Ca-lact aqueous solution, the molar ratio between the Ca^{2+}/G of alginate is equal to 25, for the concentration of 4% (w/v). Comparatively with the $CaCl_2$ for the same concentration of calcium lactate (higher molecular weight), the amount of Ca^{2+} is inferior due to the lower ion content per

molecule of this compound. However, a complete dissociation of Ca^{2+} from the lactate is not achieved. According to Kubantseva and Hartel (2002), the presence of negatively charged alcohol groups on the anion molecule causes an association between the Ca^{2+} and the lactate complex. The presence of hydroxyl groups reduces the dissociation capacity for some calcium salts. Thus, the Ca^{2+} concentration in the coagulation aqueous solution is inferior. Beyond the reduction of the Ca^{2+} content available for the alginate crosslinking, this causes also the limitation of the calcium diffusion into the MIC, leading to a less effective crosslinking and consequently to an increment of the hydrophilic active principle loss to the coagulation solution. Regarding to the calcium gluconate, the molar ratio between the Ca^{2+}/G of alginate is equal to 11, for the concentration of 4% (w/v). This represents a lower availability of Ca^{2+} ions in comparison with the $CaCl_2$ and calcium lactate solution, having the same effect already discussed on the Ca^{2+} diffusion to the MIC inner. However, in the used conditions, the Ca^{2+} from the calcium gluconate is fully dissociated in aqueous medium, which might represent an advantage comparatively with the calcium lactate.

Analyzing the overall results obtained for the EE, it can be concluded that the $CaCl_2$ is the most effective calcium source for alginate crosslinking, being followed by calcium gluconate and finally calcium lactate. From the point of view of the curcumin and safranin release profile, calcium lactate leads to a more gradual release than the other two calcium sources.

Table 35 Physico-chemical properties of alginate and the calcium sources.

Substance	**pH (*) (4% w/v)**	**pK_a**	**Molar ratio (Ca^{2+}/ G) of alginate**
Alginate	5.02	3.38 (alginate (G) unit)	-
$CaCl_2$	5.47	-7	45
Ca-glu	6.91	3.70	11
Ca-lact	6.67	3.78	25

(*) pH of the solutions prepared

5.Conclusions and future work

5. Conclusions and future work

In the present work the microencapsulation of a hydrophilic and a hydrophobic (model compounds), using alginate systems, and comparing two encapsulation methods (spray coagulation and superhydrophobic surfaces) was studied with three different calcium sources. The selected hydrophobic model active principle was curcumin and the hydrophilic one safranin; both colorants compounds. The crosslinking of the resultant microdroplets using different calcium sources was tested, in order to evaluate the effect of the crosslinker chemical structure on the alginate coagulation/gelation. Thus, calcium chloride, calcium gluconate, and calcium lactate were tested. The advantages of using superhydrophobic surfaces *versus* the conventional spray-coagulation was discussed.

The microspheres produced by the spray-coagulation technique were characterized by optical microscopy, encapsulation efficiency, dry residue, rehydration capacity, release profile, FTIR, thermogravimetric analysis and particle size. Empty microparticles were also produced for comparison. The analysis of the encapsulation efficiency revealed that when calcium chloride is used a higher encapsulation efficiency was obtained (99.25% and 98.50%, respectively for curcumin and safranin), followed by calcium gluconate (98.45% and 97.55 for curcumin and safranin) and finally calcium lactate (97.91% for curcumin and 97.42 for safranin). For curcumin, the high encapsulation efficiency registered was expected once its hydrophobic nature does not favor the migration for the aqueous coagulation solution. However, in the case of safranin the registered values were higher than expected, because its hydrophilic nature should favor its diffusion to the coagulation aqueous medium. The understanding of this phenomena must be further explored to be fully understood, namely if this occurrence can be related with the chemical nature of safranin.

Regarding the release profile, a lower level of release was achieved, for both compounds, when calcium chloride was used (5.70% of curcumin in ethanol medium, and 4.15% of safranin in distilled water), followed by the calcium gluconate crosslinked microspheres (8.3% for curcumin and 4.42% for safranin). Calcium lactate crosslinked microspheres give rise to the systems with higher release (12.1% for curcumin and 4.76% for safranin). The curcumin's release from the microspheres was limited by the curcumin crystals formation inside the microspheres, limiting its release. For safranin microspheres, a

gradual release was achieved during the evaluation period, without reaching a plateau indicating that the analysis should be extended.

The optical microscopy revealed the spherical conformation of the microspheres, while the particle size analysis showed that the larger particle size (volume distribution) was obtained with the calcium gluconate-based systems (131.46, 78.85 and 91.46 μm for curcumin, safranin and empty microspheres, respectively). The calcium chloride-base systems give rise to the smallest ones (91.65, 60.10 and 80.31 μm, respectively for curcumin, safranin and empty microspheres).

The FTIR analysis allowed the confirmation of the active principles encapsulation since the chemical contributions of both curcumin and safranin were identified on the microspheres spectra. Also, the contribution of the calcium sources used as crosslinkers was evidenced. The thermogravimetric analysis showed an increase of the thermal stability due to the alginate crosslinking, and it was also noticed that the degradation of the active principles shifted to higher temperatures due to the polymeric matrix protection.

Regarding the microparticles produced using superhydrophobic surfaces, they were characterized by optical microscopy, dry residue and rehydration capacity. During the production, a loss of the initial spherical conformation after the crosslinking addition, being this effect more visible in the curcumin microspheres. The rehydration test showed than the microspheres crosslinked with calcium gluconate have a higher capacity to rehydrate, followed by the calcium lactate ones and then the calcium chloride ones. No loss of active principle was observed by optical microscopy during the crosslinking process monitoring, which shows the advantage of this method for hydrophilic compounds encapsulation.

As future work, it would be interesting to evaluate the effects of ions resultant from the calcium sources dissociation and their influence on alginate crosslinking, particularly in the particle's structure. It would also be interesting to make a similar study using internal calcium sources for alginate crosslinking. In addition, and based on the preliminary obtained results, a more extensive study of the microencapsulation by using superhydrophobic surfaces must be performed.

6.References

6.References

Agnihotri, N., Mishra, R., Goda, C., Arora, M., 2012. Microencapsulation – A Novel Approach in Drug Delivery : A Review. J. Pharm. Sci. 2, 1–20.

Anand, P., Kunnumakkara, A.B., Newman, R.A., Aggarwal, B.B., Anand, P., Kunnumakkara, A.B., Newman, R.A., 2007. Bioavailability of Curcumin : Problems and Promises reviews Bioavailability of Curcumin : Problems and Promises. Mol. Pharmacol. 4, 807–818. https://doi.org/10.1021/mp700113r

Athira, G.K., Jyothi, A.N., 2014. Preparation and characterization of curcumin loaded cassava starch nanoparticles with improved cellular absorption. Int. J. Pharm. Pharm. Sci. 6, 171–176.

Bunn, B.J., Simpkins, N.S., 1877. Organic chemistry, Journal of the Chemical Society. Oxford University Press. https://doi.org/10.1039/js8773200725

Bustos, G., Cruz, J.M., 2012. Evaluation of Non-Conventional Coagulants to Remove Turbidity from Water 591–598. https://doi.org/10.1007/s11270-011-0884-8

Chan, L.W., Lee, H.Y., Heng, P.W.S., 2006. Mechanisms of external and internal gelation and their impact on the functions of alginate as a coat and delivery system. Carbohydr. Polym. 63, 176–187. https://doi.org/10.1016/j.carbpol.2005.07.033

Chan, L.W., Lee, H.Y., Heng, P.W.S., 2002. Production of alginate microspheres by internal gelation using an emulsification method. Int. J. Pharm. 242, 259–262. https://doi.org/10.1016/S0378-5173(02)00170-9

Ching, S.H., Bansal, N., Bhandari, B., 2017a. Alginate gel particles – A review of production techniques and physical properties. Crit. Rev. Food Sci. Nutr. 57, 1133–1152. https://doi.org/10.1080/10408398.2014.965773

Ching, S.H., Bansal, N., Bhandari, B., 2017b. Alginate gel particles–A review of production techniques and physical properties. Crit. Rev. Food Sci. Nutr. 57, 1133–1152. https://doi.org/10.1080/10408398.2014.965773

Clare, K., 2012. Algin. Ind. Gums Polysaccharides Their Deriv. Third Ed. 105–143. https://doi.org/10.1016/B978-0-08-092654-4.50010-3

Crawford, R.J., Ivanova, E.P., Webb, H.K., 2015. The Design of Superhydrophobic Surfaces, in: Superhydrophobic Surfaces. pp. 27–49. https://doi.org/10.1016/B978-0-12-801109-6.00003-3

Dabb, L.., 1971. Calcium Carbonate Dissolution and Precipitation in Water: Factors Affecting the Carbonate Saturometer Method. Utah State Univ. 1971.

Daemi, H., Barikani, M., Barmar, M., 2013. Compatible compositions based on aqueous polyurethane dispersions and sodium alginate. Carbohydr. Polym. 92, 490–496. https://doi.org/10.1016/j.carbpol.2012.09.046

Devatkal, S., Mendiratta, S.K., 2001. Use of calcium lactate with salt-phosphate and alginate-calcium gels in restructured pork rolls 58, 371–379.

Dias, M.I., Ferreira, I.C.F.R., Barreiro, M.F., 2015. Microencapsulation of bioactives for food applications. Food Funct. 6, 1035–1052. https://doi.org/10.1039/C4FO01175A

Dubey, R., Shami, T.C., Bhasker Rao, K.U., 2009. 2009 Microencapsulation technology and applications. Def. Sci. J. 59, 82–95. https://doi.org/10.14429/dsj.59.1489

Estevinho, B.N., Rocha, F., Santos, L., Alves, A., 2013. Microencapsulation with chitosan by spray drying for industry applications - A review. Trends Food Sci. Technol. 31, 138–155. https://doi.org/10.1016/j.tifs.2013.04.001

Farazuddin, M., Chauhan, A., Khan, R.M.M., Owais, M., 2011. Amoxicillin-bearing microparticles: potential in the treatment of Listeria monocytogenes infection in Swiss albino mice. Biosci. Rep. 31, 265–72. https://doi.org/10.1042/BSR20100027

Fravel, D.R., 1985. Encapsulation of Potential Biocontrol Agents in an Alginate-Clay Matrix. Phytopathology. https://doi.org/10.1094/Phyto-75-774

Galateanu, B., Dimonie, D., Vasile, E., Nae, S., Cimpean, A., Costache, M., 2012. Layer-shaped alginate hydrogels enhance the biological performance of human adipose-derived stem cells 91–95.

George, M., Abraham, T.E., 2006. Polyionic hydrocolloids for the intestinal delivery of protein drugs: Alginate and chitosan - a review. J. Control. Release 114, 1–14. https://doi.org/10.1016/j.jconrel.2006.04.017

Gharsallaoui, A., Roudaut, G., Chambin, O., Voilley, A., Saurel, R., 2007. Applications of spray-drying in microencapsulation of food ingredients: An overview. Food Res. Int. 40, 1107–1121. https://doi.org/10.1016/j.foodres.2007.07.004

Ghosal, K., Ray, S.D., 2011. Alginate/hydrophobic HPMC (60M) particulate systems: New matrix for site-specific and controlled drug delivery. Brazilian J. Pharm. Sci. 47, 833–844. https://doi.org/10.1590/S1984-82502011000400021

Ghosh, S.K., 2006. Functional coatings and microencapsulation: a general perspective, in: S.K. Ghosh (Ed.), Functional Coatings, 1st Ed., WILEY-VCH Verlag GmbH {&} Co. KGaA, Weinheim, 1–26.

Giunchedi, P., Gavini, E., Moretti, M.D., Pirisino, G., 2000. Evaluation of alginate compressed matrices as prolonged drug delivery systems. AAPS PharmSciTech 1, E19. https://doi.org/10.1208/pt010319

Goh, C.H., Wan, P., Heng, S., Chan, L.W., 2012. Alginates as a useful natural polymer for microencapsulation and therapeutic applications. Carbohydr. Polym. 88, 1–12. https://doi.org/10.1016/j.carbpol.2011.11.012

Grynkiewicz, G., Ślifirski, P., 2012. Curcumin and curcuminoids in quest for medicinal status. Acta Biochim. Pol. 59, 201–212. https://doi.org/2012_258 [pii]

Guo, Z., Liu, W., Su, B.L., 2011. Superhydrophobic surfaces: From natural to biomimetic to functional. J. Colloid Interface Sci. 353, 335–355. https://doi.org/10.1016/j.jcis.2010.08.047

Heli, H., Moosavi-Movahedi, A.A., Jabbari, A., Ahmad, F., 2007. An electrochemical study of safranin O binding to DNA at the surface. J. Solid State Electrochem. 11, 593–599. https://doi.org/10.1007/s10008-006-0204-1

Hewlings, S., Kalman, D., 2017. Curcumin: A Review of Its' Effects on Human Health. Foods 6, 92. https://doi.org/10.3390/foods6100092

Hoare, T.R., Kohane, D.S., 2008. Hydrogels in drug delivery: Progress and challenges. Polymer (Guildf). 49, 1993–2007. https://doi.org/10.1016/j.polymer.2008.01.027

Hou, J., Li, C., Guan, Y., Zhang, Y., Zhu, X.X., 2015. Enzymatically crosslinked alginate hydrogels with improved adhesion properties. Polym. Chem. 6, 2204–2213. https://doi.org/10.1039/c4py01757

Humbert, P., Przyklenk, M., Vemmer, M., Patel, A. V., 2017. Calcium gluconate as cross-linker improves survival and shelf life of encapsulated and dried Metarhizium brunneum and Saccharomyces cerevisiae for the application as biological control agents. J. Microencapsul. 34, 47–56. https://doi.org/10.1080/02652048.2017.1282550

Jang, J., Seol, Y.J., Kim, H.J., Kundu, J., Kim, S.W., Cho, D.W., 2014. Effects of alginate hydrogel cross-linking density on mechanical and biological behaviors for tissue engineering. J. Mech. Behav. Biomed. Mater. 37, 69–77. https://doi.org/10.1016/j.jmbbm.2014.05.004

Josef, E., Barat, K., Barsht, I., Zilberman, M., Bianco-Peled, H., 2013. Composite hydrogels as a vehicle for releasing drugs with a wide range of hydrophobicities. Acta Biomater. 9, 8815–8822. https://doi.org/10.1016/j.actbio.2013.06.028

Jyothi, N.V.N., Prasanna, P.M., Sakarkar, S.N., Prabha, K.S., Ramaiah, P.S., Srawan, G.Y., 2010. Microencapsulation techniques, factors influencing encapsulation efficiency. J. Microencapsul. 27, 187–197. https://doi.org/10.3109/02652040903131301

Jyothi Sri, S., Seethadevi, A., Suria Prabha, K., Muthuprasanna, P., Pavitra, P., 2012. Microencapsulation: A review. Int. J. Pharma Bio Sci. 3, P509–P531. https://doi.org/10.1007/BF00569928

Kailasapathy, K., 2002. Microencapsulation of Probiotic Bacteria 39 Microencapsulation of Probiotic Bacteria: Technology and Potential Applications. Curr. Issues Intest. Microbiol 3, 39–48.

Kampf, N., Nussinovitch, A., 2000. Hydrocolloid coating of cheeses. Food Hydrocoll. 14, 531–537. https://doi.org/10.1016/S0268-005X(00)00033-3

Koch, S., Schwinger, C., Kressler, J., Heinzen, C., Rainov, N.G., 2003. Alginate encapsulation of genetically engineered mammalian cells: Comparison of production devices, methods and microcapsule characteristics. J. Microencapsul. 20, 303–316. https://doi.org/10.1080/0265204021000058438

Kragovic, M., Dakovic, A., Markovic, M., Petkovic, A., 2016. Kinetic of thermal degradation of alginate-zeolite composites. Zast. Mater. 57, 559–564. https://doi.org/10.5937/ZasMat1604559K

Kubantseva, N., Hartel, R.W., 2002. Solubility of calcium lactate in aqueous solution. Food Rev. Int. 18, 135–149. https://doi.org/10.1081/FRI-120014355

Lee, K.Y., Mooney, D.J., 2012. Alginate: Properties and biomedical applications. Prog. Polym. Sci. 37, 106–126. https://doi.org/10.1016/j.progpolymsci.2011.06.003

Lee, P., Rogers, M.A., 2012. Effect of calcium source and exposure-time on basic caviar spherification using sodium alginate. Int. J. Gastron. Food Sci. 1, 96–100. https://doi.org/10.1016/j.ijgfs.2013.06.003

Leick, S., Henning, S., Degen, P., Suter, D., Rehage, H., 2010. Deformation of liquid-filled calcium alginate capsules in a spinning drop apparatus. Phys. Chem. Chem. Phys. 12, 2950–2958. https://doi.org/10.1039/b921116k

Li, X.-M., Reinhoudt, D., Crego-Calama, M., 2007. What do we need for a superhydrophobic surface? A review on the recent progress in the preparation of superhydrophobic surfaces. Chem. Soc. Rev. 36, 1350. https://doi.org/10.1039/b602486f

Lima, A.C., Batista, P., Valente, T.A.M., Silva, A.S., Correia, I.J., Mano, J.F., 2013. Novel Methodology Based on Biomimetic Superhydrophobic Substrates to Immobilize Cells and Proteins in Hydrogel Spheres for Applications in Bone Regeneration. Tissue Eng. Part A 19, 1175–1187. https://doi.org/10.1089/ten.tea.2012.0249

Lima, A.C., Correia, C.R., Oliveira, M.B., Mano, J.F., 2014. Sequential ionic and thermogelation of chitosan spherical hydrogels prepared using superhydrophobic surfaces to immobilize cells and drugs. J. Bioact. Compat. Polym. 29, 50–65. https://doi.org/10.1177/0883911513513660

Lima, A.C., Song, W., Blanco-Fernandez, B., Alvarez-Lorenzo, C., Mano, J.F., 2011. Synthesis of temperature-responsive Dextran-MA/PNIPAAm particles for controlled drug delivery using superhydrophobic surfaces. Pharm. Res. 28, 1294–1305. https://doi.org/10.1007/s11095-011-0380-2

Lin, J.K., 2007. Molecular targets of curcumin, Advances in Experimental Medicine and Biology. https://doi.org/10.1007/978-0-387-46401-5_10

Mandal, S., Senthil Kumar, S., Krishnamoorthy, B., Basu, S.K., 2010. Development and evaluation of calcium alginate beads prepared by sequential and simultaneous methods. Brazilian J. Pharm. Sci. 46, 785–793. https://doi.org/10.1590/S1984-82502010000400021

Martins, A., Barros, L., Carvalho, A.M., Santos-Buelga, C., Fernandes, I.P., Barreiro, F., Ferreira, I.C.F.R., 2014. Phenolic extracts of Rubus ulmifolius Schott flowers: characterization, microencapsulation and incorporation into yogurts as nutraceutical sources. Food Funct. 5, 1091–1100. https://doi.org/10.1039/C3FO60721F

Matté, G.M., Da Rosa, S., 2013. a Tecnologia Da Microencapsulação Através Das Microesferas De Quitosana. Rev. Iberoam. Polímeros Vol. Iberoam. Polim 14, 206–218. https://doi.org/10.1017/CBO9781107415324.004

Mchugh, D.J., 2013. Chapter 2 - Production, Properties and Uses of Alginates 1–42.

Meier, M., 2015. Microencapsulação : Inovação em diferentes áreas.

Mondal, S., Ghosh, S., Moulik, S.P., 2016. Stability of curcumin in different solvent and solution media: UV–visible and steady-state fluorescence spectral study. J. Photochem. Photobiol. B Biol. 158, 212–218. https://doi.org/10.1016/j.jphotobiol.2016.03.004

Mørch, Ý. a., Donati, I., Strand, B.L., 2006. Effect of Ca 2+ , Ba 2+ , and Sr 2+ on Alginate Microbeads. Biomacromolecules 7, 1471–1480. https://doi.org/10.1021/bm060010d

Nosonovsky, M., Bhushan, B., 2009. Superhydrophobic surfaces and emerging applications: Non-adhesion, energy, green engineering. Curr. Opin. Colloid Interface Sci. 14, 270–280. https://doi.org/10.1016/j.cocis.2009.05.004

Papadopoulou, S.K., Tsioptsias, C., Pavlou, A., Kaderides, K., Sotiriou, S., Panayiotou, C., 2011. Superhydrophobic surfaces from hydrophobic or hydrophilic polymers via nanophase separation or electrospinning/electrospraying. Colloids Surfaces A Physicochem. Eng. Asp. 387, 71–78. https://doi.org/10.1016/j.colsurfa.2011.07.028

Paques, J.P., Van der Linden, E., Van Rijn, C.J.M., Sagis, L.M.C., 2013. Alginate submicron beads prepared through w/o emulsification and gelation with CaCl2 nanoparticles. Food Hydrocoll. 31, 428–434. https://doi.org/10.1016/j.foodhyd.2012.11.012

Patel, N., Lalwani, D., Gollmer, S., Injeti, E., Sari, Y., Nesamony, J., 2016. Development and evaluation of a calcium alginate based oral ceftriaxone sodium formulation. Prog. Biomater. 5, 117–133. https://doi.org/10.1007/s40204-016-0051-9

Pathak, T.S., Yun, J.H., Lee, J., Paeng, K.J., 2010. Effect of calcium ion (cross-linker) concentration on porosity, surface morphology and thermal behavior of calcium alginates prepared from algae (Undaria pinnatifida). Carbohydr. Polym. 81, 633–639. https://doi.org/10.1016/j.carbpol.2010.03.025

Paulo, F., Santos, L., 2017. Design of experiments for microencapsulation applications: A review. Mater. Sci. Eng. C 77, 1327–1340. https://doi.org/10.1016/j.msec.2017.03.219

Pawar, H., 2014. Phytochemical Evaluation and Curcumin Content Determination of Turmeric Rhizomes Collected From Bhandara District of Maharashtra (India). Med. Chem. (Los. Angeles). 4, 588–591. https://doi.org/10.4172/2161-0444.1000198

Pawar, S.N., Edgar, K.J., 2012. Alginate derivatization: A review of chemistry, properties and applications. Biomaterials 33, 3279–3305. https://doi.org/10.1016/j.biomaterials.2012.01.007

Poncelet, D., Poncelet De Smet, B., Beaulieu, C., Huguet, M.L., Fournier, A., Neufeld, R.J., 1995. Production of alginate beads by emulsification/internal gelation. II. Physicochemistry. Appl. Microbiol. Biotechnol. 43, 644–650. https://doi.org/10.1007/BF00164768

Priyadarsini, K.I., 2014. The chemistry of curcumin: From extraction to therapeutic agent. Molecules 19, 20091–20112. https://doi.org/10.3390/molecules191220091

Puga, A.M., Lima, A.C., Mano, J.F., Concheiro, A., Alvarez-Lorenzo, C., 2013. Pectin-coated chitosan microgels crosslinked on superhydrophobic surfaces for 5-fluorouracil encapsulation. Carbohydr. Polym. 98, 331–340. https://doi.org/10.1016/j.carbpol.2013.05.091

Puliyalil, H., Filipič, G., Uroš Cvelbar, 2015. Recent Advances in the Methods for Designing Superhydrophobic Surfaces, in: Surface Energy. pp. 312–333. https://doi.org/http://dx.doi.org/10.5772/60852

Quinlan, E., López-Noriega, A., Thompson, E.M., Hibbitts, A., Cryan, S.A., O'Brien, F.J., 2017. Controlled release of vascular endothelial growth factor from spray-dried alginate microparticles in collagen–hydroxyapatite scaffolds for promoting vascularization and bone repair. J. Tissue Eng. Regen. Med. 11, 1097–1109. https://doi.org/10.1002/term.2013

Rached, I., Barros, L., Fernandes, I.P., Santos-Buelga, C., Rodrigues, A.E., Ferchichi, A., Barreiro, M.F., Ferreira, I.C.F.R., 2016. Ceratonia siliqua L. hydroethanolic extract obtained by ultrasonication: antioxidant activity, phenolic compounds profile and effects in yogurts functionalized with their free and microencapsulated forms. Food Funct. 7, 1319–1328. https://doi.org/10.1039/C6FO00100A

Rakesh, P., Vipin, K., Kanchan, K., 2015. Alginate Beads Prepared by Ionotropic Gelation Technique : Formulation Design 5, 45–47.
Ramachandran, S., Fontanille, P., Pandey, A., Larroche, C., 2006. Gluconic acid: Properties, applications and microbial production. Food Technol. Biotechnol. 44, 185–195.

Rao, J. K., & Rao, K.P., 1997. Controlled Release of FITC-BSA from Polymer Coated Gelatin Microspheres. J. Bioact. Compat. Polym. 12, 127–139. https://doi.org/978-1-61804-022-0 384

Roach, P., Shirtcliffe, N.J., Newton, M.I., 2008. Progess in superhydrophobic surface development. Soft Matter 4, 224–240. https://doi.org/10.1039/B712575P

Rodrigues, S.N., Martins, I.M., Fernandes, I.P., Gomes, P.B., Mata, V.G., Barreiro, M.F., Rodrigues, A.E., 2009. Scentfashion®: Microencapsulated perfumes for textile application. Chem. Eng. J. 149, 463–472. https://doi.org/10.1016/j.cej.2009.02.021

Rouillard, A.D., Berglund, C.M., Lee, J.Y., Polacheck, W.J., Tsui, Y., Bonassar, L.J., Kirby, B.J., 2011. Methods for Photocrosslinking Alginate Hydrogel Scaffolds with High

Cell Viability. Tissue Eng. Part C Methods 17, 173–179. https://doi.org/10.1089/ten.tec.2009.0582

Russo, R., Malinconico, M., Santagata, G., 2007. Effect of cross-linking with calcium ions on the physical properties of alginate films. Biomacromolecules 8, 3193–3197. https://doi.org/10.1021/bm700565h

Schaller, C.P., 2008. Concepts of Acids and Bases.

Silva, C.M., Ribeiro, A.J., Figueiredo, I.V., Gonçalves, A.R., Veiga, F., 2006. Alginate microspheres prepared by internal gelation: Development and effect on insulin stability. Int. J. Pharm. 311, 1–10. https://doi.org/10.1016/j.ijpharm.2005.10.050

Silva, P.T. da, Fries, L.L.M., Menezes, C.R. de, Holkem, A.T., Schwan, C.L., Wigmann, É.F., Bastos, J. de O., Silva, C. de B. da, 2014. Microencapsulation: concepts, mechanisms, methods and some applications in food technology. Ciência Rural 44, 1304–1311. https://doi.org/10.1590/0103-8478cr20130971

Silva, M.M., Lidon, F.C., 2016. An overview on applications and side effects of antioxidant food additives 28, 823–832. https://doi.org/10.9755/ejfa.2016-07-806

Singh, M.N., Hemant, K.S.Y., Ram, M., Shivakumar, H.G., 2010. Microencapsulation: A promising technique for controlled drug delivery. Res. Pharm. Sci. 5, 65–77. https://doi.org/10.1155/2014/926157

Soccol, C.R., Vandenberghe, L.P.S., Rodrigues, C., 2006. New Perspectives for Citric Acid Production and Application. Food Technol. Biotechnol. 44, 141–149. https://doi.org/1330-9862

Song, S., Wang, Z., Qian, Y., Zhang, L., Luo, E., 2012. The Release Rate of Curcumin from Calcium Alginate Beads Regulated by Food Emulsi fi ers. J. Agric. Food Chem. 60, 4388–4395. https://doi.org/dx.doi.org/10.1021/jf3006883 |

Song, W., Lima, A.C., Mano, J.F., 2010. Bioinspired methodology to fabricate hydrogel spheres for multi-applications using superhydrophobic substrates. Soft Matter 6, 5868. https://doi.org/10.1039/c0sm00901f

Straub, D.A., 2007. Nutrition in Clinical Practice Calcium Supplementation in Clinical Practice : A Review of 286–296. https://doi.org/10.1177/0115426507022003286

Strimpakos, A.S., Sharma, R.A., 2008. Curcumin: Preventive and Therapeutic Properties in Laboratory Studies and Clinical Trials. Antioxid. Redox Signal. 10, 511–546. https://doi.org/10.1089/ars.2007.1769

Stuart, B., 2004. Infrared Spectroscopy: Fundamentals and Applications, 1st ed. John Wiley and Sons, Sydney, Australia.

Subhash Latthe, S., Basavraj Gurav, A., Shridhar Maruti, C., Shrikant Vhatkar, R., 2012. Recent Progress in Preparation of Superhydrophobic Surfaces: A Review. J. Surf. Eng. Mater. Adv. Technol. 02, 76–94. https://doi.org/10.4236/jsemat.2012.22014

Szekalska, M., B, A.P., N, E.S., Ciosek, P., Winnicka, K., 2016. Alginate : Current Use and Future Perspectives in Pharmaceutical and Biomedical Applications 2016. https://doi.org/10.1155/2016/7697031

Tam, S.K., Dusseault, J., Bilodeau, S., Langlois, G., Hallé, J.P., Yahia, L., 2011. Factors influencing alginate gel biocompatibility. J. Biomed. Mater. Res. - Part A 98 A, 40–52. https://doi.org/10.1002/jbm.a.33047

Topuz, F., Henke, A., Richtering, W., Groll, J., 2012. Magnesium ions and alginate do form hydrogels: a rheological study. Soft Matter 8, 4877. https://doi.org/10.1039/c2sm07465f

Trailokya, A., Srivastava, A., Bhole, M., Zalte, N., 2017. Calcium and calcium salts. J. Assoc. Physicians India 65, 100–103.

Tsai, F.H., Kitamura, Y., Kokawa, M., 2017. Liquid-core alginate hydrogel beads loaded with functional compounds of radish by-products by reverse spherification: Optimization by response surface methodology. Int. J. Biol. Macromol. 96, 600–610. https://doi.org/10.1016/j.ijbiomac.2016.12.056

Tsuiji, K., 2001. Microencapsulation of pesticides and their improved handling safety. J. Microencapsul. 18, 137–147. https://doi.org/10.1080/026520401750063856

Viegas, J., Barros, L., Fernandes, I., Ferreira, I.C.F.R., Barreiro, F., 2013. Application of spray-coagulation method to microencapsulate catechin having in view cosmetic, pharmaceutical or nutraceutical areas. pp. 1–2.

Viegas, J.S., 2013. Encapsulação de um extrato hidroalcoólico de Rosa micrantha Borrer ex Sm para fins alimentares 86.

Xiu, Y., Zhu, L., Hess, D., Wong, C.P., 2006. Superhydrophobic silicone/PTFE films for biocompatible application in encapsulation of implantable microelectronics devices. Proc. - Electron. Components Technol. Conf. 2006, 686–692. https://doi.org/10.1109/ECTC.2006.1645731

Zheng, B., Zhang, Z., Chen, F., Luo, X., McClements, D.J., 2017. Impact of delivery system type on curcumin stability: Comparison of curcumin degradation in aqueous

solutions, emulsions, and hydrogel beads. Food Hydrocoll. 71, 187–197. https://doi.org/10.1016/j.foodhyd.2017.05.022

Appendices

Appendix A

Table A1 Production of safranin microspheres crosslinked with the different calcium sources (Assay nº1)

	Assay Nº1				
Calcium source	**Weight of wet MIC (mg)**	**Weight of dry MIC (mg)**	**EE (%, (w/w))**	**Load (w/w)**	**Dry Residue % (w/w)**
$CaCl_2$	1168.5	113.5	98.365	0.1093	9.71
Ca-glu	1267.1	127.2	98.001	0.1089	10.04
Ca-lact	1215.1	108.4	97.543	0.1084	9.67

Table A2- Production of safranin microspheres crosslinked with the different calcium sources (Assay nº2)

	Assay Nº2				
Calcium source	**Weight of wet MIC (mg)**	**Weight of dry MIC (mg)**	**EE (%, (w/w))**	**Load (w/w)**	**Dry Residue % (w/w)**
$CaCl_2$	982.2	91.2	98.728	0.1097	9.29
Ca-glu	1141.1	104.2	97.901	0.1088	9.13
Ca-lact	975.0	104.1	97.424	0.1082	10.68

Table A3- Production of curcumin microspheres crosslinked with the different calcium sources (Assay Nº1)

	Assay Nº1				
Calcium source	**Weight of wet MIC (mg)**	**Weight of dry MIC (mg)**	**EE (%, (w/w))**	**Load (w/w)**	**Dry Residue % (w/w)**
$CaCl_2$	837.5	61.7	99.136	0.1102	7.06
Ca-glu	921.3	92.5	98.236	0.1092	9.25
Ca-lact	946.3	75.7	97.537	0.1084	8.00

Table A4- Production of safranin microspheres crosslinked with the different calcium sources (Assay Nº2)

	Assay Nº2				
Calcium source	**Weight of wet MIC (mg)**	**Weight of dry MIC (mg)**	**EE (%, (w/w))**	**Load (w/w)**	**Dry Residue % (w/w)**
$CaCl_2$	971.2	98.7	99.930	0.1104	10.16
Ca-glu	1012.1	112.2	98.744	0.1097	11.09
Ca-lact	988.2	115.8	98.116	0.1090	11.72